Structural Visualization of HECT-E3 Ufd4 accepting and transferring Ubiquitin to Form K29/K48-branched Polyubiquitination on N-degron

Junxiong Mao[1,3], Huasong Ai[1,2,3], Xiangwei Wu[1,3], Qingyun Zheng[2*], Hongyi Cai[1], Lujun Liang[1], Zebin Tong[1], Man Pan[2]*, Lei Liu[1*]

[1]Tsinghua-Peking Joint Center for Life Sciences, MOE Key Laboratory of Bioorganic Phosphorus Chemistry and Chemical Biology, Department of Chemistry, Tsinghua University, Beijing 100084, China.

[2]Institute of Translational Medicine, National Center for Translational Medicine (Shanghai), School of Chemistry and Chemical Engineering, Shanghai Jiao Tong University, Shanghai, 200240, China.

[3]These authors contributed equally to this work: Junxiong Mao, Huasong Ai, Xiangwei Wu.

[*]Correspondence author:

Lei Liu, lliu@mail.tsinghua.edu.cn;

Man Pan, panman@sjtu.edu.cn;

Qingyun Zheng, zheng_qy@sjtu.edu.cn .

Summary

Proteins with destabilizing N-terminal residues are degraded via K48-linked ubiquitination-dependent N-degron pathway, during which the HECT-type E3 ligase Ufd4 can further augment polyubiquitination events on these proteins to accelerate their degradation. How Ufd4 increase polyubiquitination on ubiquitinated N-degrons remains unclear. Here, we biochemically determined that Ufd4 preferentially ubiquitinates the proximal ubiquitin in K48-linked ubiquitin chain in K29-linkage specific manner and revealed high-resolution cryo-EM structures of Ufd4 accepting (E2-to-E3 state, 3.52 Å) and transferring ubiquitin-thioester (E3-to-substrate state, 3.31 Å) , respectively. The N-terminal ARM region and HECT domain C-lobe of Ufd4 were identified and characterized as key structural elements that together recruit K48-linked diUb and orient Lys29 of its proximal Ub to the active cysteine of Ufd4 for K29-linked branched ubiquitination. These structures not only provide mechanistic insights into the architecture of the Ufd4 complex but also show the full picture of the Ub transferring cascades of HECT-type E3 ligase.

Keywords

N-degron pathway, ubiquitination, HECT-type E3 ligase, Cryo-EM, Chemical trap strategy, Ub transferring cascades.

Introduction

The N-end rule pathway is the first ubiquitin (Ub)-dependent proteolytic system identified that targets proteins with destabilizing residues (basic residues or bulky hydrophobic residues) at the N-terminus for ubiquitination-dependent degradation[1,2]. An expanded body of work in the last three decades has characterized a range of N-end rule pathways, such as the Arg/N-degron pathway, Ac/N-degron pathway, and Pro/N-degron pathway, and revealed their critical roles in regulating multiple physiological processes including DNA damage repair, cell cycle, and apoptosis[3-5]. Disturbance of the N-end rule pathway has been shown to induce the accumulation of misfolded proteins and consequent proteotoxicity, which underlies human diseases such as Johanson-Blizzard syndrome[6]. The universally present N-end rule degradation pathway has also been exploited for developing new cancer therapeutics via N-degron-based proteolysis-targeting chimeras (PROTACs)[7].

Prior to proteasomal degradation, substrate proteins with destabilizing residues at the N-terminus (termed as N-degrons) are often recognized by UBR family E3 ligases and ubiquitinated in a K48 linkage-specific manner[8]. This ubiquitination process on N-degron substrates can be further augmented by another E3 ligase Ufd4 (a K29-linkage-specific HECT-type E3 ligase), leading to accelerated substrate degradation[9,10]. The mechanism of a representative yeast Ubr1-catalyzed process, including the initiation of N-degron ubiquitination and the K48 linkage-specific elongation step, was recently elucidated by cryo-electron microscopy (cryo-EM) studies in our group[11]. Nonetheless, the mechanism through which Ufd4 introduces K29-linked Ub chains on substrates to increase the processivity of polyubiquitination remains unknown.

Mechanistic studies on E3 ligases have been challenging due to the dynamic nature of the transient intermediate complexes in ubiquitin transfer[12-14]. Covalently linked mimics of E2-substrate or E2-Ub-substrate conjugates have recently been developed to trap RING-type E3 ligases in their catalytic conformation, as exemplified in studies on the Ubr1[11], Cullin-RING ubiquitin ligases (CRLs)[13,15], and APC/C systems[12]. Despite these advances, how ubiquitin transfer occurs during HECT-type E3 catalytic cascades had yet to be visualized. Here, we developed a mechanism-based chemical trapping strategy and captured structural snapshots of the HECT-type E3 ligase Ufd4 in both the E2-to-E3 and E3-to-substrate Ub transfer cascades. Our work

revealed the mechanism by which Ufd4 assembles K29/48 branched ubiquitin chain to increase the polyubiquitylation processivity on substrates in the Arg/N-degron pathway and has shown the full picture of the Ub transferring cascades of HECT-type E3 ligase.

Results

Ufd4 prefers to ubiquitinate the proximal Lys29 of K48-linked ubiquitin chains

Previous studies have shown that Ubr1/Ufd4 together strengthened the ubiquitination and degradation of the substrate (e.g., Scc1[10] and the O6meG-DNA alkyltransferase Mgt1[9]) through K29- and K48-linked polyubiquitin chains, in which Ufd4 has been proposed to be a potential E4-like enzyme and act as a ubiquitin chain elongation factor[16]. Accordingly, we began our study with the reconstitution of Ufd4-mediated polyubiquitination reactions on the substrates of monoUb, K29-linked diUb, or K48-linked diUb using the yeast Ub-activating enzyme (E1) Uba1, the Ub-conjugating enzyme (E2) Ubc4, the HECT-type E3 ligase Ufd4, and wild-type (WT) Ub. Polyubiquitination was observed to be enhanced on K48-linked diUb compared to monoUb or K29-linked diUb **(Figures 1A and S1A)**. The enzymatic kinetics of Ufd4 on K48-linked diUb were faster than those on monoUb by 4.2-fold (0.021 μM/min vs. 0.005 μM/min) **(Figure 1B)**. Furthermore, Ufd4 ubiquitination assays on different lengths of K48-linked ubiquitin chains (di-, tri-, tetra-, and penta-) suggested that the polyubiquitination efficiency escalated with increasing chain length **(Figure S1B)**.

To examine the linkage specificity of the ubiquitin chain generated by Ufd4, we performed polyubiquitination reactions with Uba1, Ubc4, Ufd4, fluorescence-labeled monoubiquitinated degron peptide (Ub-degron) substrate, and seven lysine-to-arginine (K6R, K11R, K27R, K29R, K33R, K48R, or K63R) mutated Ub. Consistent with the previous results, when Ub-K29R was used instead of other Ub mutants, the substrate polyubiquitination on Ub-degron was significantly reduced **(Figure S2A)**. Mass spectrometric analysis of the polyubiquitin on Ub-degron generated by Ufd4 using WT Ub showed that the major linkage type was Lys29 (93%) **(Figure S2B)**.

Next, the topology of the ubiquitin chains generated by Ufd4 on K48-linked ubiquitin substrates was determined. The Ufd4-mediated K29-linked polyubiquitination activity on K48-linked ubiquitin substrates was significantly reduced when Ub-K29R was used instead of other Ub mutants as detected by Ub chain-specific western blot **(Figures S1C-S1F)**[17]. Mass spectrometry analysis of the polyubiquitin chains generated by Ufd4 on K48-linked diUb suggested the formation of K29/K48-linked branched chains **(see Supplementary Text, Figures 1C-1E)**[18,19]. To compare the difference in the Ufd4-catalyzed ubiquitination of K48-linked diUb at the proximal or distal Lys 29, we prepared K48-linked diUb with mutation of lysine to cysteine at either proximal or distal K29 site (named $diUb^{K48prox*}$ and $diUb^{K48dist*}$). The efficiency of the Ufd4 assembly of ubiquitin chains on $diUb^{K48dist*}$ was 1.46-fold faster than that on $diUb^{K48prox*}$ (0.0073 μM/min vs. 0.0050 μM/min) **(Figures 1F and 1G)**, indicating a preference for proximal Lys29. Taken together, these biochemical results suggest that Ufd4 preferentially ubiquitinates the proximal Lys29 of K48-linked ubiquitin chains.

Visualization of the substrate (K48-linked diUb) ubiquitination catalyzed by Ufd4

To investigate the molecular mechanism of how Ufd4 transfers its thioester-bound Ub to the proximal Lys29 of the K48-linked diUb substrate, we covalently linked the active site of Ufd4 (Cys1450), the C-terminus of Ub and the proximal Lys29 of K48-linked diUb to form a stable complex to mimic the corresponding transition state **(Figure 2A)**. This complex was prepared in two steps: first, an engineered K29/48 branched triUb probe (named $triUb^{probe}$) was synthesized according to our previously reported procedure[20-22], in which the proximal Ub of K48-linked diUb was chemically ligated with the donor Ub **(Figures S3A and S3C)**; then, $triUb^{probe}$ was cross-linked with Ufd4 in an active site (Cys1450)-dependent manner to form the designed stable complex mimic **(Figure S3E)**. This complex was subjected to single-particle cryo-EM analysis. A total of 5,332 micrographs were collected and processed to obtain a cryo-EM map at a global resolution of 3.31 Å **(Table S1 and Figures S4A-S4D)**. The map quality allowed unambiguous docking and atomic modeling of the complex **(Figures S5A and S5B)**.

The overall structure of Ufd4 with donor Ub conjugated on proximal Lys29 of K48-linked diUb (named $Ufd4\text{-}triUb^{K29/K48}$) resembles a closed ring shape in

which Ufd4 forms a clamp sandwiching donor Ub and K48-linked diUb **(Figures 2C and 2D)**. The visible Ufd4 scaffold consists of three regions: the armadillo-like (ARM) region (163-706) composed of multiple repeating α-helices, the HECT domain that contains the N-lobe (1097-1361) and C-lobe (1361-1483), and the multihelix region (MHR) (707-1097) bridging the two regions mentioned above **(Figures 2B-2D)**. The ubiquitin module contains two globular parts: the K48-linked diUb and the donor Ub. K48-linked diUb was bound by the HECT domain C-lobe and two helical repeats of the ARM region, which we termed Ub-interacting helical clusters (UIHC1, residues 263-301; UIHC2, residues 304-332) **(Figure 2B)**. The donor Ub binds to the HECT domain C-lobe and its C-terminus is oriented toward the Ufd4-active Cys1450. The N-terminal region of Ufd4 (1-162), which was reported to interact with the proteasome[23], is invisible in our cryo-EM map.

Ufd4 binds the substrate (K48-linked diUb) through multidentate interfaces

The contact between Ufd4 and K48-linked diUb can be subdivided into interactions with proximal ubiquitin (named $Ub^{K48\text{-}prox}$) and distal ubiquitin (named $Ub^{K48\text{-}dist}$) **(Figure 3A)**. $Ub^{K48\text{-}dist}$ is bound by the Ufd4 UIHC1 and UIHC2 motifs through multiple hydrophobic interactions. Specifically, residues Tyr276, Ile277 and Asp278 of Ufd4 UIHC1 are located close to the Leu8 loop of $Ub^{K48\text{-}dist}$, and the side chain of Phe313 of UIHC2 inserts into the hydrophobic pocket of $Ub^{K48\text{-}dist}$ formed by Ile44, His68, and Val70 **(Figures 3B and S5E and S6B)**, which often participate in recruiting Ub-binding proteins[24-27]. $Ub^{K48\text{-}prox}$ is bound by UIHC2 and the HECT C-lobe, where residues Thr315, Ile316 and His317 of UIHC2 are directed toward residue Arg54 of $Ub^{K48\text{-}prox}$ **(Figures 3C and S5F)**, and residues His1378 and His1433 of the HECT domain C-lobe are pointed toward the hydrophilic surface formed by $Ub^{K48\text{-}prox}$ residues Pro19 and Ser20 **(Figures 3D, S5G and S6C)**. The dual anchoring effect of UIHC2 and the HECT C-lobe on $Ub^{K48\text{-}prox}$ orients its Lys29 side chain toward the active cysteine of Ufd4 (distance between α-carbon atoms is 9.04 Å, **Figure S6D**). Together, these interactions with Ufd4 reshape K48-linked diUb to adopt an unprecedented extended conformation that differs from prior structures determined for either free K48-linked diUb or in complex with various recognition proteins (e.g., Rpn13, SARS PLpro, MINDY1) **(Figure S6A)**[24-26]. According to the relative orientation between these two Ub units, the

K48 sidechain of $Ub^{K48\text{-}prox}$ was directed toward the C-terminus of $Ub^{K48\text{-}dist}$ **(Figure S6E)**, underlying the structural basis of the Ufd4 substrate selectivity on the K48-linked Ub chain.

The importance of the above key interacting surfaces was assessed by assaying the effects of mutations in UICH1, UIHC2, and the HECT domain C-lobe of Ufd4. In Ufd4-mediated polyubiquitination of K48-linked diUb, the Ufd4 UIHC1 triple mutant (Y276A/I277A/D278A, named the YID mutant) slows down the activity by 25% **(Figure S6G)**. The Ufd4 UIHC2 triple mutant (F313A/T315A/I316A, named FTI mutant) or single mutant H317A impairs the activity of Ufd4 by 90% or 70%, respectively **(Figures S6F and S6G)**. The HECT domain C-lobe H1433A mutant reduced activity by a quarter **(Figure S6F)**.

Interactions between the HECT domain C-lobe and the donor Ub

The donor Ub was positioned by the helix (1462-1475) and loop (1433-1445) of the Ufd4 HECT domain C-lobe **(Figures 3E and S7A)**. In the Ufd4 helix (1462-1475), the residues Arg1468 and Gln1471 point toward the Leu8 loop of donor Ub. In the loop (1433-1445), residues Asp1436, Leu1438 and Glu1442 are close to the donor Ub hydrophobic interface formed by Ile36 and Leu71 **(Figures 3F and S5H)**. The Ufd4 R1468A mutant in the helix (1462-1475) almost completely eliminated the ubiquitination activity **(Figures S7C and S7E)**. The Ufd4 E1442A mutant or double mutant (D1436A/L1438A, named DL mutant) in the loop (1433-1445) weakened the activity by approximately 30% or 50%, respectively **(Figure S7E)**. Ufd4 ubiquitination assay with donor Ub mutants (I36A or L71A) shows reduced activity by 50% or 90% **(Figure S7D)**. Simultaneous mutations of Ufd4 and donor Ub (i.e., Ufd4 DL and Ub I36A pair, or Ufd4 E1442A and Ub L71A pair) resulted in negligible ubiquitination activity **(Figure S7F)**. Notably, the above interaction positions the C-terminal thioester of the donor Ub proximal to the K29 side chain of $Ub^{K48\text{-}dist}$, underlying the structural insight into Ufd4-catalyzed K29-linked branched ubiquitination on K48-linked Ub chain**(Figures 3G-H)**.

We further compared the structural organization of the C-lobe and donor Ub in our Ufd4-triUb$^{K29/K48}$ structure with the Ub-charged HECT ligase structure (case shown by Nedd4, PDB code: 4bbn)[28], and the HECT E3~Ub-substrate

complex structure (case shown by Nedd4 yeast homolog Rsp5, PDB code: 4lcd) **(Figure S7B)**[29]. The conformation of donor Ub relative to the C-lobe changes in our structures, Glu34 of the donor Ub in our structure flips 40.3° (4bbn) and 42.8° (4lcd) relative to C-lobe Gln1471 (measured by the α carbon atoms) and undergoes shifts of 15.66 Å (4bbn) and 15.97 Å (4lcd), respectively, suggesting the plasticity of the Ub conformation in the substrate ubiquitination by different HECT E3 ligases.

Visualization of Ufd4 charging Ub from Ubc4~Ub thioester

To obtain a comprehensive view of the catalytic cascade of Ufd4, we determined the structure of Ufd4 accepting Ub thioester from Ubc4~Ub thioester. Thus, the active site of Ufd4, the C-terminus of ubiquitin and the active site of Ubc4 were chemically linked by a two-step method **(Figure 4A)**. An activity-based probe that relies on a chemically engineered Ubc4-Ub (named Ubc4-Ub^{probe}) was first synthesized and then crosslinked with Ufd4 in an active center (Cys1450)-dependent manner to form a stable complex mimic **(Figures S3B, S3D and S3F)**. The mimic was subjected to cryo-EM analysis and provided three cryo-EM reconstructions, including a 3.52 Å map in which Ub and Ufd4 (1-706) were invisible (termed Ufd4$^{\triangle ARM}$-Ubc4), a 4.30 Å map in which Ub and Ufd4 (1-162) were invisible (termed Ufd4-Ubc4), and a 6.39 Å map in which only Ufd4 (1-706) was invisible (termed Ufd4$^{\triangle ARM}$-Ubc4-Ub) **(Table S1 and Figures S8A-S8F)**. The map quality allowed unambiguous docking and atomic modeling of the complex **(Figures S5C and S5D)**.

The main difference observed for the three structures above is the visibility of the Ub and Ufd4 ARM regions, and in all three structures, the Ufd4 HECT domain interacts with Ubc4 through its N and C lobes **(Figure S9A)**. Detailed structural analysis of Ufd4 with Ubc4 was then performed by focusing on the Ufd4$^{\triangle ARM}$-Ubc4 structure at the highest resolution (3.52 Å). Our Ufd4$^{\triangle ARM}$-Ubc4 structure superimposes well with the previous HECT E3-E2 structure (case shown by Nedd4-UbcH5b, PDB code:3JW0)[30] with an average root-mean-square deviation (RMSD) of 0.89 Å **(Figure S9B)**, suggesting an overall similar HECT E3-E2 interaction pattern.

In the structure, Ubc4 is embraced by the Ufd4 HECT domain C-lobe and N-lobe **(Figure 4B)**. The contacts between the Ufd4 HECT domain N-lobe and Ubc4 are contributed by multiple interfaces. The Ubc4 residue Phe63, a highly

conserved residue among many other HECT E3 ligases (e.g., E6AP[31] and Nedd4L[30]), inserts into the hydrophobic groove consisting of Leu1262, Leu1266, Pro1286, Thr1287, and Tyr1313 **(Figures 4D and S5J)**. The Ubc4 F63A mutant almost completely diminished the activity **(Figure S9D)**. The interaction between the Ufd4 HECT domain C-lobe and Ubc4 involves the pairing of C lobe residue H1433 with Ubc4 residue His126 and the pairing of C lobe residue H1378 with Ubc4 residues Val121, Pro122, and Glu123 **(Figures 4C and S5I)**. Ufd4 (H1433A, H1378A) or Ubc4 (V121A/P121A, E123A) mutants reduced E3~Ub thioester formation **(Figures S9D and S9E)**. Three other interactions are presented: the N-lobe residue Tyr1167 and Ubc4 residues Pro58, Pro65, and Lys64, the N-lobe residue Asp1292 and Ubc4 residue Ser3, and the N-lobe residue Ser1283 and Ubc4 residue Arg6 **(Figures 4E, 4F, S5K and S5L)**. Mutations of Ufd4 (Y1167A) and Ubc4 (P58A/P65A, S3A) decrease the E3~Ub thioester formation efficiency **(Figures S9D and S9E)**.

The transition from transthiolation to K29-linked Ub assembly

The two structures we have resolved above correspond to the HECT E3 enzyme E2-to-E3 transthiolation state (Ufd4-Ubc4-Ub complex structures) and the E3-to-substrate ubiquitination state (Ufd4-triUb$^{K29/K48}$ complex structure). The similarities and differences between these two conformations were analyzed to investigate the interdomain conformational changes of the HECT E3 enzyme in different states.

First, we focused on the conformational differences of Ufd4 in recruiting E2 (Ubc4) and substrate (K48-linked diUb). The structures of Ufd4-Ubc4 (which contains the ARM region) and Ufd4-triUb$^{K29/K48}$ were compared, and the Ufd4 MHR (707-1097) and the N-lobe (1361-1483) superimpose well in these two structures with an average RMSD of 0.99 Å **(Figure 5A)**. Notably, the ARM region (163-706) in the two structures undergoes conformational changes; for instance, the Ufd4 residue Glu184 undergoes a 28.41 Å shift and a 14.8° deflection of Glu184 relative to the residue His715. This ARM conformational change of Ufd4 at different steps of the catalytic cascade implies that regions outside the HECT domain play a previously unidentified role in substrate recognition in ubiquitin transfer.

Next, we compared the structures of Ufd4$^{\triangle ARM}$-Ubc4 (the structure at the highest resolution), Ufd4-triUb$^{K29/K48}$ and apo Ufd4 (predicted by AlphaFold, AF-P33202-F1) to identify the conformational changes in the HECT domain of Ufd4 in different catalytic states. The structural organization of the HECT domain N-lobe in these three structures remains unchanged during state transitions **(Figure S9F)**. Interestingly, the conformation of the HECT domain C-lobe in Ufd4$^{\triangle ARM}$-Ubc4 (transthiolation process) is significantly changed compared with the other two structures, where His1378 of the C-lobe is shifted by 45.91 Å and flipped relative to Ile1357 of the N-lobe by 75.3° **(Figures 5B and 5C**). Notably, this conformational change was observed to be stabilized by an interaction formed between residue Lys1152, Thr1183, Arg1224 of the N lobe and residue I1417 on the hinge of the C lobe (1411–1418) **(Figure 5F)**, the latter of which undergoes a 17.63 Å shift and a 99.0° deflection (relative to Asp1356 of the N-lobe in Ufd4-triUb$^{K29/K48}$ structure) from the original position in binding with residue Ile1357 to this new position **(Figures 5D and 5E)**. When Ile1417 was mutated to Gly1417, an in vitro ubiquitination assay and an E3~Ub thioester charging assay showed that the elongation of the K29-linked Ub chain on the K48-linked diUb was significantly impaired in the I1417G mutant Ufd4 compared to WT **(Figure S9C)**, and the E3 thioester formation efficiency of this mutant Ufd4 was reduced to 20% **(Figure S9E)**, suggesting that the conformational change of the HECT domain C-lobe is required for the transthiolation process.

Finally, the Ufd4 C-lobe residues His1378 and H1433 were found to interact with both Ubc4 and K48-linked diUb in the Ufd4$^{\triangle ARM}$-Ubc4 and Ufd4-triUb$^{K29/K48}$ structures, respectively **(Figures 3D and 4C)**, indicating that Ubc4 needs to disassociate beforehand and the C-lobe reorientates to provide space for interactions with K48-linked diUb during the ubiquitination process.

Validation of key interactions between K29/K48-linked triUb and Ufd4

To investigate the effect of the key interfaces observed in our structures on K48-ubiquitinated substrates, a 44-mer type-1 degron peptide and a truncated substrate Scc1(residues 268-384) were used in the Ufd4-mediated polyubiquitination assay[11]. The K48-linked ubiquitin chains were preassembled on these two substrates using Ubr1 and its E2 enzyme Ubc2, and further elongated by Ufd4 and its mutants. The ubiquitination results

showed that WT Ufd4 could further extend the polyubiquitin chain on the type-1 degron peptide as well as the bona fide substrate Scc1$^{268-384}$, while the ubiquitin chain elongating activity was substantially reduced by the Ufd4 mutants FTI, R1468A, and H317A **(Figures S10A and S10B)**.

To validate the structural mechanism in a physiological setting, a previously developed yeast growth assay was performed[9]. In S. cerevisiae, the ubiquitination level of Mgt1 is regulated by both Ufd4 and Ubr1, and its degradation leads to yeast death[9]. We constructed a Ufd4 knockout yeast strain, and complementation with Ufd4 and its mutants altered Mgt1 ubiquitination levels, thus affecting the growth status of yeast **(Figure 6A)**. When WT Ufd4 was added to compensate for the Ufd4-knockout strain, the yeast strain exhibited poor growth, and the addition of the DNA-alkylating agent MNNG further inhibited yeast growth **(Figure 6B)**. These results were consistent with previous in vivo degradation experiments showing that the Mgt1 level was affected by Ufd4 and the DNA-alkylating agent[9]. Complementation with Ufd4 mutants (FTI, R1468A, or H317A) decelerated yeast death compared to WT Ufd4 with or without the addition of MNNG **(Figure 6B)**, indicating that the Ufd4 and K29/K48-linked triUb interfaces also affect the stabilization of substrates in vivo.

Discussion

In the Arg/N-end rule pathway, N-degrons are targeted by Ubr1 to assemble K48-linked chains, and Ufd4 can augment the processivity of polyubiquitylation by introducing K29-linked Ub chains to accelerate substrate degradation *in vivo* (such as Mgt1)[9,10]. The human homolog of Ufd4, TRIP12, has been reported to facilitate PROTAC molecule-driven targeted degradation by generating K29/K48-branched ubiquitin chains[32]. Our biochemical and quantitative mass spectrometry experiments clarified major aspects of the molecular mechanism of Ufd4, in which Ufd4 preferentially ubiquitinates the proximal Lys29 site on K48-linked Ub chains **(Figures 1A, 1B and S1A-S1F)**. To gain structural insight into this mechanism, we designed mechanism-based chemical trapping strategies for the study of HECT E3-specific processes, namely, the transfer of Ub from E2 to E3 and subsequently from E3 to the substrate, providing a complete mechanistic understanding of how Ubr1 and Ufd4 cooperatively mediate the ubiquitination of N-degrons.

Based on the structures of Ufd4-mediated ubiquitin charging and ubiquitin transfer to the proximal Lys29 site of K48-linked diUb, we proposed a functional model representing the whole catalytic process of Ufd4. First, Ubc4~Ub is recruited by the HECT N-lobe and C-lobe of Ufd4, followed by the conformational rotation of the HECT C-lobe to accept Ub from Ubc4 and discharge Ubc4. Subsequently, the conformation of the ARM region reorientates to sandwich the K48-linked diUb substrate together with the HECT C-lobe, which directs the proximal Lys29 residue of K48-linked diUb toward Ufd4 catalytic Cys1450. Finally, the ubiquitin thioester transfers from Ufd4 catalytic Cys1450 to the proximal Lys29 of K48-linked diUb **(Figure 6C)**.

Previous research has revealed how RING and RBR-type ligases orchestrate E2 enzymes to enable polyUb chain assembly[11,12,14,33]. For example, the requirements for the monoubiquitination and Ub chain elongation of RING-type E3 ligase APC/C are satisfied by multisite interactions between its cullin-RING core and the specialized placement of E2 enzyme UBE2C or UBE2S, respectively[12]. Zinc finger insertions embedded within the RING2 domain of the RBR-type E3 ligase RNF216 contribute to its Ub chain elongation specificity[33]. Nevertheless, the understanding of the functional mechanism of the HECT E3 ligase is still limited. Here, we provide the first comprehensive investigation of how HECT-type E3 ligase (i.e., Ufd4) coordinates acceptor Ub to assemble polyUb chains on K48-linked diUb. The HECT domain C-lobe and the non-HECT domain ARM regions coordinately recognize the K48-linked diUb, directing Lys29 of the proximal UbK48 toward the Ufd4 active center. Moreover, the HECT domain C-lobe undergoes significant conformational changes in the E2-to-E3 state and the E3-to-substrate state to orchestrate HECT-type E3-mediated Ub transfer cascades.

Finally, our work advances the knowledge of linkage-specific polyUb chain assembly. Previous studies on the formation of M1-linked, K48-linked, and K63-linked Ub chains show that Ub-binding domains are required to orientate the acceptor Ub to enable linkage specificity assemblies, such as a zinc finger region embedded within HOIP RING2[34], the UBA and the UBC domain of UBE2K[14]. Here, we showed that Ufd4 UIHC2 and the HECT C-lobe can work cooperatively to localize the Lys29 residue on the proximal Ub of the K48-linked diUb toward the Ufd4 Cys1450 active center **(Figure S6D)**, providing the first model for K29-linked Ub chain elongation.

Acknowledgments

We thank the Tsinghua University Branch of China National Center for Protein Sciences (Beijing) for cryo-EM sample screening in 200 kV Tecnai Arctica, and cryo-EM data collection in 300 kV Titan Krios microscopy. Funding: National Key R&D Program of China (2022YFC3401500 to L. L.). National Natural Science Foundation of China (22137005, 92253302, and 22227810 to L. L.; 22277073 and 92253302 to M. P.). XPLORER prize (to L. L.). Shanghai Rising-Star Program (22QA1404900 to M. P.). Shanghai Pilot Program for Basic Research - Shanghai Jiao Tong University (21TQ1400224 to M. P.). H. A. thanks the funding by the National Facility for Translational Medicine (Shanghai).

Author contributions

Conceptualization: J. M., H. A., Q. Z., M. P., and L. L. Design of experiments: J. M., H. A., and L. L. Synthesis of E2-to-E3 transthiolation intermediate mimics: J. M. Synthesis of E3-to-substrate ubiquitination intermediate mimics: X. W. and J. M. Cryo-EM sample preparation: J. M., X. W., and H. A. Structural determination of cryo-EM structures of Ufd4-triUb$^{K29/48}$ and Ufd4 in complex with Ubc4-Ub: H. A. Synthesis of fluorescently labelled K48-linked diUb and Ub: J. M., and X.W. Cloning and purification of E1, Ufd4, Ubc4, and all their mutants: J. M., X.W., H. C., J. L., and Z. T. Ufd4-related in vitro enzymatic assays and yeast assays: J. M., X.W., and H.C. Ufd4-related western-blot assays: Q. Z. and J. M. Identification the topology of polyubiquitin chains generated by Ufd4 on K48-linked diUb: J. M. and Q. Z. The manuscript writing: J. M., H. A., X. W., M. P., and L. L. The project supervision: M. P., and L. L.

Competing interests

The authors declare no competing interests.

Data and materials availability

The cryo-EM maps and corresponding atomic coordinates have been deposited in the Electron Microscopy Data Bank (EMDB) and Protein Data Bank (PDB) under accession codes EMD-35929, 8J1P (Ufd4-triUb$^{K29/48}$); EMD-35931, 8J1R (Ufd4 in complex with Ubc4~Ub). Data for mass spectrometry characterization of recombinant or semisynthetic proteins used in this study are provided in **Supplementary Chemistry Files. 1-8**. Uncropped gels and blots are provided in **Supplementary Source data**. All data are

available in the main text or the supplementary materials. Newly created materials from this study may be requested from the corresponding authors.

Methods

Cloning and plasmid construction

The plasmid encoding *S. cerevisiae Ufd4* gene was synthesized by GenScript (Nanjing, China), and its codon was optimized for *S. cerevisiae* and *Escherichia coli* (*E.coli*) overexpression, respectively. For overexpression by *S. cerevisiae*, the *Ufd4* gene was subcloned to the vector YEplac181 containing an N-terminal DYKDDDDK (Flag) tag. For overexpression by *E. coli*, the gene was inserted between the BamHI and EcoRIsites of the vector pGEX-4T-1 with an N-terminal GST tag followed by an HRV 3C protease cleavage site. The DNA sequence encoding yeast (*S. cerevisiae*) *Ubc4* was synthesized by GenScript and its codon was optimized for *E. coli* overexpression. The gene was further cloned into the vector pET-28a with an N-terminal His tag followed by an HRV 3C protease cleavage site. Different *Ufd4* and *Ubc4* mutants were constructed by site-directed mutagenesis. The DNA sequences of wild-type Ub and Ub mutants including Ub-K6R, Ub-K11R, Ub-K27R, Ub-K33R, Ub-K48R, Ub-K63R, Ub-G76C, Ub-K29R/K48R, Ub-K29C/K48R, Ub-77D (a Ub variant with an additional amino acid Asp at the C terminus), Ub-K29C/77D, and Ub-MCQ (Ub variant with an additional amino acid Cys between Met1 and Gln2) were constructed and cloned to the vector pET-22b by GenScript (Nanjing, China). The plasmids containing *S. cerevisiae Uba1*, *S. cerevisiae Ubc2*, *S. cerevisiae Ubr1*, and the truncated *S. cerevisiae* genes *Scc1* (268–384; also known as MCD1) were the same as previously used[11].

Protein expression and purification

Ufd4 used for cryo-EM sample and its mutants used in Ufd4-triUb$^{K29/K48}$ complex structure-related ubiquitination assay were expressed in yeast and purified in a similar manner to yeast Ubr1 as previously described[11]. In brief, plasmids containing *Ufd4* and its mutants were transformed into yeast (BY4741) cells. Single colonies were selected to grow in a synthetic medium with Leu defective resistance (SC, −Leu) to an optical density at 600 nm (OD_{600}) of 2-3. The yeast cells were collected by centrifugation at 4,000 r.p.m. and then fully resuspended with lysis buffer (50 mM HEPES, pH 7.5, 150 mM NaCl, protease inhibitor cocktail (Roche), and 10% glycerol). The suspension liquid was frozen into small balls and subsequently ground into a fine powder using a freezing grinder (SPEX Sample Prep 6870 Freezer/Mill). The powder was defrosted in ice water and centrifuged at 12000 r.p.m. for 1 h. The

supernatant was loaded on the anti-Flag affinity resin (Thermo Fisher Scientific, A36803) and incubated at 4 ℃ for 2h. After washing adequately, 1 mg/mL Flag peptide dissolved in buffer (50 mM HEPES, pH 7.5, 150 mM NaCl) was used to elute Flag-tagged Ufd4. Ufd4 was then purified by ion exchange (Mono Q anion exchange column, GE Healthcare) with buffer A containing 50 mM HEPES, pH 8.0 and buffer B containing 50 mM HEPES, pH 7.5, 1 M NaCl. Samples at indicated peaks were concentrated and further purified using size exclusion chromatography (Superose 6 column, GE Healthcare) with a buffer containing 50 mM HEPES, pH 7.5, and 150 mM NaCl. Finally, Ufd4 was analyzed by SDS-PAGE (LabPAGE 4-12% 15 Wells, LABLEAD).

The purification of Ubc2, Ubc4 and its variants were the same as previously described[11]. Briefly, plasmids containing *Ubc4* and its variants were introduced into E. coli BL21(DE3) competent cells and cultured in Luria Broth (LB) medium with 20 μg/mL kanamycin at 37 ℃ to OD_{600} of 0.6. The cells were cooled to 18℃ and induced by 0.4 mM isopropylβ-d-1-thiogalactopyranoside (IPTG) for 16h. The cells were centrifuged at 4000 r.p.m. for 25 min at 4 °C and the precipitate was fully resuspended with lysis buffer (50 mM HEPES, pH 7.5, 150 mM NaCl and 1 mM phenylmethyl sulfonyl fluoride (PMSF)). After lysed by sonication and 12000 r.p.m. centrifugation, the supernatant was incubated with Ni-NTA affinity column for 2 h at 4 °C. After washing with at least 10 column volumes of lysis buffer (50 mM HEPES, pH 7.5, 150 mM NaCl, 20 mM imidazole), the proteins were eluted with a lysis buffer containing 400 mM imidazole and further purified with size exclusion chromatography (Superdex 200 column, GE Healthcare) with a buffer containing 50 mM HEPES, pH 7.5, and 150 mM NaCl. The expression of Ufd4 used in the Ufd4/Ubc4-Ub complex structure-related ubiquitination assay was similar to Ubc4 as we described above. Differently, after lysis by sonication and high-speed centrifugation, the supernatant was incubated with Glutathione beads for 2 h at 4℃. The protein was eluted with a lysis buffer containing 30 mM Glutathione. The elution was incubated with HRV 3C protease overnight to remove GST tag and further purified as described above for yeast-expressed Ufd4. Scc1(268–384) and Uba1 were obtained as we used before[11]. Wild-type (WT) Ub and Ub mutants were purified as previously described[20].

Yeast growth assay

S. cerevisiae strain lacking *Ufd4* (*ΔUfd4*) in the BY4741 background was constructed by Thermo Fisher Scientific. Ufd4 mutants (R1468A, FTI mutant,

H317A) were constructed in the context of the vector YEplac181, carrying the wild-type Ufd4.

Yeast strains lacking Ufd4 were plated in a rich (YPD) solid medium containing 2% agarose and 2% glucose (w/v) and grown at 30 ℃ for 2 days. Single colonies were selected to grow in a YPD liquid medium at 30 ℃ to mid-log-phase (OD_{600} of 0.4-0.8). Yeast cultures were centrifuged at 3000 r.p.m. for 10min and washed with double-distilled H_2O. Centrifuged again and resuspended with 1 x TE buffer (10 mM Tris-HCl, pH 8.0, 1 mM Ethylene Diamine Tetraacetic Acid (EDTA)). Repeated again and resuspended with 1x LiAc (100 mM LiAc, pH 7.5) and 0.5x TE buffer to obtain *ΔUfd4* competent yeast cells and stored on ice for further use. WT Ufd4 and its mutants (R1468A, FTI mutant, H317A) were transformed to *ΔUfd4* competent cells and plated in SC (−Leu) medium containing 2% agarose and 2% glucose (w/v) at 30℃ for 2 days.

Single colonies of the yeast strains mentioned above were selected to grow in SC (−Leu) medium containing 2% glucose at 30℃ overnight. Dilute with SC (−Leu) medium to OD_{600} of 0.4 and grow at 30°C for 2 h until OD_{600} of 1.0. Add N-methyl-N'-nitro-N-nitrosoguanidine (MNNG) stock solution (50 mM NaOAc, pH 5.0, 6 mM MNNG) to the final concentration of 60 μM and grow at 30°C for 1 h As previously described[9]. Single colonies were spotted in serial fivefold dilution onto the SC (−Leu) plates. The plates were grown at 30°C for 2 days before imaging.

Preparation of K29-linked and K48-linked Ub chains

K29-linked chains were obtained with 0.2 μM Uba1, 4 μM Ubc4, 0.5 μM Ufd4, and 200 μM WT Ub at 30°C in the reaction buffer (50 mM HEPES, pH 7.5, 150 mM NaCl, 10 mM $MgCl_2$ and 5 mM ATP). K48-linked chains were obtained with 1 μM Uba1, 20 μM Ube2K and 800 μM WT Ub at 30°C in the same reaction buffer. For K48-linked diUb variants, WT Ub was substituted with Ub mutants: $diUb^{K48prox*}$ (200 μM Ub-K29C/77D and 200 μM Ub-K48R); $diUb^{K48dist*}$ (200 μM Ub-77D and 200 μM Ub-K29C/K48R); K48 diUb used for kinetic assay (200 μM Ub-G76C and 200 μM Ub-K48R). The reactions were terminated by buffer (50 mM NaOAc, pH 4.5) and K29-linked and K48-linked chains were separated by ion exchange (MonoS cation column, GE Healthcare) with buffer A containing 50 mM NaOAc, pH 4.5 and buffer B containing 50 mM NaOAc, pH 4.5, 1 M NaCl. Samples at indicated peaks were

collected and then dialyzed into a buffer containing 50 mM HEPES, pH 7.5 and 150 mM NaCl, for further use.

Preparation of fluorescently labeled substrates

Ub-MCQ, Ub-G76C, diUb^{K48prox}*, diUb^{K48dist}* and K48 diUb used for kinetic assay were obtained as described above. For the labeling reaction, 1.5 eq. of fluorescein-5-maleimide (Invitrogen, F150) was added to 2 mg Ub mutants or K48-linked diUb variants, and the mixtures were incubated at room temperature for 20 min. The labeled proteins were purified with size-exclusion chromatography (Superdex 200 column, GE Healthcare) with a buffer containing 50 mM HEPES, pH 7.5, 150 mM NaCl.

***In vitro* Ubiquitination assay**

In vitro ubiquitination assays were performed with 0.2 μM Uba1, 4 μM Ubc4, 0.25 μM Ufd4, 10 μM substrate Ub chains (K29-linked diUb, K48-linked diUb/triUb/tetraUb/pentaUb) or 2 μM fluorescently labeled substrates (fluorescent Ub-G76C, K48-diUb, diUb^{K48prox}*, diUb^{K48dist}*) and 80 μM WT Ub at 30°C in the reaction buffer (50 mM HEPES, pH 7.5, 150 mM NaCl, 10 mM $MgCl_2$ and 5 mM ATP).

To measure the ubiquitination activity on K48-linked substrate peptide and real N-end rule substrate, another ubiquitination assays were performed with 0.2 μM Uba1, 4 μM Ubc2, 0.25 μM Ubr1, 4 μM Ubc4, 0.25 μM Ufd4, 80 μM Ub, 5 μM (fluorescent degron, synthesized previously[11]) or 10 μM Scc1 (268–384) at 30 °C with the same reaction buffer mentioned above.

These reactions was terminated by adding 4 x sodium dodecyl sulfate (SDS) sample buffer, and then analyzed using SDS-PAGE and visualized by Coomassie Brilliant blue dye/fluorescence or visualized by western blot using K29 linkage-specific antibodies[17] and K48 linkage-specific antibodies (Abcam, ab190061). For the ubiquitination assays to validate key structural interfaces, the same concentrations of Ufd4 and Ub variants (Ub-L8A, Ub-I36A, Ub-L71A) were used in the assay as the respective wild type.

Kinetic measurement of Ub transfer on Ub, K48di, diUb^{K48prox}* and diUb^{K48dist}*

To measure the ubiquitination velocity between Ub and K48-linked diUb or between diUb^{K48prox}* and diUb^{K48dist}*, a time-resolved kinetic experiment was

performed. *In vitro* ubiquitination assays were performed as described above, and mixtures were sampled and terminated by 4× SDS sample buffer at indicated time points (0, 1, 2, 5, 10, 15, 25, 45, 60 min). Then analyzed using SDS-PAGE and imaged by fluorescence. Data from three replicates were quantified by image lab (Bio-Rad software) and time rate curves of ubiquitination were plotted.

Transthiolation assay with fluorescently labelled Ub-MCQ

Transthiolation assay consists of two operational steps. First, 0.1 μM Uba1, 5 μM Ubc4 or its variants, 10 μM fluorescently labelled Ub-MCQ were mixed at 30°C for 5 min in the reaction buffer (50 mM HEPES, pH 7.5, 150 mM NaCl, 10 mM $MgCl_2$ and 5 mM ATP) to generate fluorescent ubiquitin-loaded Ubc4 or it variants and then terminated with a final concentration of 250 mM EDTA (pH 7.4) on ice. Next, the loaded Ubc4 or its variants was reacted with Ufd4 or its variants to the following final concentrations: Ubc4 or its variants, 1.25 μM; fluorescent ubiquitin, 2.5 μM; Ufd4 or its variants, 0.5 μM and mixtures were sampled and terminated by 4× SDS sample buffer without Dithiothreitol (DTT) at 30s. Then analyzed using SDS-PAGE and imaged by fluorescenceat (Bio-Rad).

Mass spectrometry analysis of polyubiquitin chains

To obtain polyubiquitin chains generated by Ufd4 on K48-linked chains, *in vitro* ubiquitination assay was performed as described above. The reaction was quenched with 25 mM EDTA on ice. Then added 5 μM engineered viral protease Lbpro* and incubated at 37°C overnight.

The identification and quantification of ubiquitin variants digested by Lbpro* were described as before[19]. In brief, diluted the reaction to 1 μM ubiquitin with a buffer (50 mM HEPES, pH 7.5, 150 mM NaCl). To perform high-mass protein analysis, samples were analyzed on a Q-TOF mass spectrometer (SYNAPT G2-Si, Waters company) instrument. The raw native electrospray mass spectra can be further deconvoluted by MaxEnt 1 (Waters) to generate a spectrum (relative intensity versus mass). This spectrum allows a single species to transform all the charge-state peaks into a single (zero-charge) peak. Microsoft Excel to further process the spectrum, and the intensities of un- (8,451.65 Da), single- (8,565.69 Da), and double-modified (8,679.73 Da) ubiquitin were exported.

To identify the K29 site and K48 site double-modified ubiquitin, the reaction digested after Lbpro* was further treated with a low concentration of WaLP (Gene, P8113L), a serine protease secreted from the soil bacteria Lysobacter enzymogenesis that can specifically hydrolyze peptide bonds after Tyr, Val, Ala, Ser, and Met, at 4 °C for 2 h[18]. The identification of the peptides was performed as previously described[35]. To analyze the specific linkage, a Thermo-Dionex Ultimate 3000 HPLC system was used and peptides were separated by a 60 min gradient elution at a flow rate of 0.3 μL/min. This system allows direct interface with the Thermo Orbitrap Fusion mass spectrometer. To identify the peptide segments, a Proteome Discovery searching algorithm (version 1.4) was used to search against the selected database derived from the MS/MS spectra of each LC-MS run.

Generation of the probe capturing the transition state of the K29 linkage assembly on K48-linked diUb

Preparation of $Ub_{(1–76)}$-MesNa

The$Ub_{(1–76)}$ hydrazine with a biotin tag at the N-terminus (1.0 equiv), prepared through protein chemical synthesis as previously described[36], was dissolved in -15 °C ligation buffer (2 mL, 100 mM NaH_2PO_4, 6 M Gn-HCl, pH 2.3). Then, $NaNO_2$ (10 equiv) was added to the reaction, and the reaction was stirred for 30 min at -15 °C. After that, 2-mercaptoethanesulfonate(MesNa, 50 equiv) was added to the reaction and the pH was slowly adjusted to 5.0-5.5. Next, The reaction reacted at room temperature for 3-4 hours. Finally, ligation buffer was added to dilute the reaction before purification, and the product was purified by semi-preparative HPLC using a Welch Ultimate XB-C4 column (21.2 × 150 mm, 5 μm particle size) and lyophilized.

Preparation of K48 diUb-CAET-SAcm

1mM $diUb^{K48dist}$* with 40 mM (2-((2-chloroethyl)amino)ethane-1-(Sacetaminomethyl)thiol) were incubated in alkylation buffer (6 M Gn-HCl, 0.2 M HEPES, 10 mM TCEP, pH=8.0-8.5) at 30°C for overnight. The desired product was isolated by RP-HPLC and lyophilized.

Preparation of K48 diUb-CAET-SH

Lyophilized K48 diUb-CAET-SAcm (final concentration 1 mM) was dissolved in reaction buffer (6 M Gn-HCl, 0.2 M NaH_2PO_4 buffer, pH 7.4). Next, fresh $PdCl_2$

(15 equiv) was added to the reaction and the reaction was incubated at 30°C for 2-3 h. Finally, The reaction was quenched by adding DTT at a final concentration of 1 mM, and then the product was purified by semi-preparative HPLC and lyophilized.

Preparation of K29/48 branched triUb-SH

Lyophilized K48 diUb-CAET-SH (1.0 equiv.) was dissolved in reaction buffer (6 M Gn-HCl, 100 mM NaH_2PO_4, Ph 7.4) to a final concentration of 1 mM. Next, 4-mercaptophenylacetic acid (MPAA, 50 equiv.) and $Ub_{(1–76)}$-MesNa(1.5 equiv.) were added to the reaction buffer and the pH was adjusted to 6.5. Then, the reaction mixture was stirred at room temperature overnight, and the product was purified by semi-preparative HPLC and lyophilized.

Preparation of K29/48 branched triUb probe

Lyophilized K48/29-triUb (1.0 equiv.) was dissolved in 1 mL buffer containing 6 M guanidinium chloride, 0.1 M NaH_2PO_4 buffer, pH 7.4 at a final concentration of 2 mg/mL. Then, 2,2′-Dipyridyl disulfide (AT_2, 25 equiv.) was added to the buffer and the reaction mixture was stirred at room temperature for 2 h. Finally, the desired probe was purified and refolded with a Superdex75 column (GE Healthcare) pre-equilibrated with 50 mM HEPES, pH 8.0, 150 mM NaCl.

Generation of the probe capturing the transition state of the Ufd4-Ubc4 transthiolation

Preparation of $Ub_{(1–75)}$-MesNa

The $Ub_{(1–75)}$ hydrazine was prepared from Ub-G76C as previously described[37] and was dissolved in -15 °C ligation buffer (2 mL, 100 mM NaH_2PO_4, 6 M Gn-HCl, pH 2.3). $NaNO_2$(10 equiv)and 2-mercaptoethanesulfonate (MesNa, 50equiv) were then added to the reaction sequentially, as in the preparation of $Ub_{(1–76)}$-MesNa. Finally, ligation buffer was added to dilute the reaction before purification, and semi-preparative HPLC and lyophilized purified the product.

Preparation of Ubc4-CAET-SAcm

1mM Ubc4 mutant with only one Cys at C86 (Ubc4 C only) with 40 mM (2-((2-chloroethyl)amino)ethane-1-(Sacetaminomethyl)thiol) were incubated in alkylation buffer (6 M Gn-HCl, 0.2 M HEPES, 10 mM TCEP, pH = 8.0-8.5) at

30°C for overnight. The desired product was isolated by RP-HPLC and lyophilized.

Preparation of Ubc4-CAET-SH

Lyophilized Ubc4-CAET-SAcm (final concentration 1 mM) was dissolved in reaction buffer (6 M Gn·HCl, 0.2 M NaH_2PO_4 buffer, pH 7.4). Next, fresh $PdCl_2$ (15 equiv) was added to the reaction and the reaction was incubated at 37°C for 2-3h. Finally, The reaction was quenched by adding DTT at a final concentration of 1 mM, and then the product was purified by semi-preparative HPLC and lyophilized.

Preparation of Ubc4-Ub-SH

Lyophilized Ubc4-CAET-SH (1.0 equiv.) was dissolved in reaction buffer (6 M Gn-HCl, 100 mM NaH_2PO_4, Ph 7.4) to a final concentration of 1 mM. Next, 4-mercaptophenylacetic acid (MPAA, 50 equiv.) and $Ub_{(1–75)}$-MesNa(1.5 equiv.) were added to the reaction buffer and the pH was adjusted to 6.5. Then, the reaction mixture was stirred at room temperature overnight, and the product Ubc4-Ub was purified by semi-preparative HPLC and lyophilized.

Preparation of Ubc4-Ub probe

Lyophilized Ubc4-Ub (1.0 equiv.) was dissolved in 1 mL buffer containing 6 M guanidinium chloride, 0.1 M NaH_2PO_4 buffer, pH 7.4 at a final concentration of 1.5 mg/mL. Then, 25 equiv. AT_2 (2,2′-Dipyridyl disulfide) was added to the buffer and the reaction mixture was stirred at room temperature for 2 h. Finally, the desired product, Ubc4-Ub probe, was purified and refolded with Superdex75 column pre-equilibrated with 50 mM HEPES, pH 8.0, 150 mM NaCl.

Sample preparation for single-particle cryo-EM

1.5 equiv K29/48 branched triUb probe, or Ubc4-Ub probe was mixed with Ufd4 (0.6 mg/mL) and incubated at 30 °C in a water bath for 30 min. Prior to grid freezing using a Vitrobot mark IV (Thermo Fisher Scientific) running at 8°C and 100% humidity, 0.0001% fluorinated octyl maltoside (final concentration) was added to the samples. A volume of 3.5 µL sample were applied to glow-discharged Quantifoil Au 1.2/1.3 grids for 1 min and blotted for 1 s or 3 s, then immersed in liquid ethane to freeze.

Cryo-EM Data collection and image processing

A total of 5,332 (Ufd4-triUb$^{K29/K48}$ dataset), and 3,404 (Ufd4/Ubc4~Ub dataset) cryo-EM micrographs were collected on a 300 kV Titan Krios microscope equipped with a Gatan K3 direct electron detector camera. Images were recorded using AutoEmation 2.0 at a pixel size of 1.074 Å with a total of 50 electrons over 32 frames. The defocus was set in a range of -1.5 µm to -2.0 µm. MotionCor2 (v. 1.2.6)[42] and Gctf (v. 1.88) [43] were used for motion correction and CTF parameter estimation. All the data were processed on RELION (v. 3.1)[44] for particle picking, 2D classification, 3D classification, mask generation, refinement, postprocessing, and polishing. The detailed processing workflow can be found in Extended Data Figure 5 (Ufd4-triUbK29/48 dataset) and Extended Data Figure 9 (Ufd4/Ubc4~Ub dataset).

Model building, refinement and validation

The cryo-EM maps of the Ufd4-triUb$^{K29/K48}$ complex and Ufd4/Ubc4~Ub complex sharped at different B-factors were used for model building. The AlphaFold predicted Ufd4 structure (code: AF-P33202-F1), ubiquitin (PDB code: 1UBQ) and Ubc4 (PDB code: 1QCQ) were fitted into the cryo-EM maps with rigid-body refinement in UCSF ChimeraX (v. 1.2.5) [45]. The individual models were merged into one molecule in WinCoot (V. 0.8.2) [46]. Real-space refinement in Phenxi (1.19.2) [47] was subsequently carried out with secondary structure constraints and/or geometry restraints. Further iterative manual visualization and adjustment were conducted to give the final models. The statistics model building, refinement and validation were summarized in Table S1. Structural analysis and figure layout were prepared in ChimeraX (v. 1.2.5).

References

1. Bachmair, A., Finley, D., and Varshavsky, A. (1986). In vivo half-life of a protein is a function of its amino-terminal residue. Science *234*, 179-186. https://doi.org/10.1126/science.3018930.
2. Chau, V., Tobias, J.W., Bachmair, A., Marriott, D., Ecker, D.J., Gonda, D.K., and Varshavsky, A. (1989). A Multiubiquitin Chain Is Confined to Specific Lysine in a Targeted Short-Lived Protein. Science *243*, 1576-1583. https://doi.org/10.1126/science.2538923.
3. Bartel, B., Wünning, I., and Varshavsky, A. (1990). The recognition component of the N-end rule pathway. Embo j *9*, 3179-3189. https://doi.org/10.1002/j.1460-2075.1990.tb07516.x.
4. Hwang, C.S., Shemorry, A., and Varshavsky, A. (2010). N-terminal acetylation of cellular proteins creates specific degradation signals. Science *327*, 973-977. https://doi.org/10.1126/science.1183147.
5. Chen, S.J., Wu, X., Wadas, B., Oh, J.H., and Varshavsky, A. (2017). An N-end rule pathway that recognizes proline and destroys gluconeogenic enzymes. Science *355*. https://doi.org/10.1126/science.aal3655.
6. Zenker, M., Mayerle, J., Lerch, M.M., Tagariello, A., Zerres, K., Durie, P.R., Beier, M., Hülskamp, G., Guzman, C., Rehder, H., et al. (2005). Deficiency of UBR1, a ubiquitin ligase of the N-end rule pathway, causes pancreatic dysfunction, malformations and mental retardation (Johanson-Blizzard syndrome). Nat Genet *37*, 1345-1350. https://doi.org/10.1038/ng1681.
7. Lee, Y., Heo, J., Jeong, H., Hong, K.T., Kwon, D.H., Shin, M.H., Oh, M., Sable, G.A., Ahn, G.O., Lee, J.S., et al. (2020). Targeted Degradation of Transcription Coactivator SRC-1 through the N-Degron Pathway. Angew Chem Int Ed Engl *59*, 17548-17555. https://doi.org/10.1002/anie.202005004.
8. Tasaki, T., Sriram, S.M., Park, K.S., and Kwon, Y.T. (2012). The N-end rule pathway. Annu Rev Biochem *81*, 261-289. https://doi.org/10.1146/annurev-biochem-051710-093308.
9. Hwang, C.S., Shemorry, A., and Varshavsky, A. (2009). Two proteolytic pathways regulate DNA repair by cotargeting the Mgt1 alkylguanine transferase. Proc Natl Acad Sci U S A *106*, 2142-2147. https://doi.org/10.1073/pnas.0812316106.
10. Hwang, C.S., Shemorry, A., Auerbach, D., and Varshavsky, A. (2010). The N-end rule pathway is mediated by a complex of the RING-type Ubr1 and HECT-type Ufd4 ubiquitin ligases. Nat Cell Biol *12*, 1177-1185. https://doi.org/10.1038/ncb2121.
11. Pan, M., Zheng, Q., Wang, T., Liang, L., Mao, J., Zuo, C., Ding, R., Ai, H., Xie, Y., Si, D., et al. (2021). Structural insights into Ubr1-mediated N-degron polyubiquitination. Nature *600*, 334-338.

https://doi.org/10.1038/s41586-021-04097-8.
12. Brown, N.G., VanderLinden, R., Watson, E.R., Weissmann, F., Ordureau, A., Wu, K.P., Zhang, W., Yu, S., Mercredi, P.Y., Harrison, J.S., et al. (2016). Dual RING E3 Architectures Regulate Multiubiquitination and Ubiquitin Chain Elongation by APC/C. Cell *165*, 1440-1453. https://doi.org/10.1016/j.cell.2016.05.037.
13. Baek, K., Krist, D.T., Prabu, J.R., Hill, S., Klügel, M., Neumaier, L.M., von Gronau, S., Kleiger, G., and Schulman, B.A. (2020). NEDD8 nucleates a multivalent cullin-RING-UBE2D ubiquitin ligation assembly. Nature *578*, 461-466. https://doi.org/10.1038/s41586-020-2000-y.
14. Nakasone, M.A., Majorek, K.A., Gabrielsen, M., Sibbet, G.J., Smith, B.O., and Huang, D.T. (2022). Structure of UBE2K-Ub/E3/polyUb reveals mechanisms of K48-linked Ub chain extension. Nat Chem Biol *18*, 422-431. https://doi.org/10.1038/s41589-021-00952-x.
15. Horn-Ghetko, D., Krist, D.T., Prabu, J.R., Baek, K., Mulder, M.P.C., Klügel, M., Scott, D.C., Ovaa, H., Kleiger, G., and Schulman, B.A. (2021). Ubiquitin ligation to F-box protein targets by SCF-RBR E3-E3 super-assembly. Nature *590*, 671-676. https://doi.org/10.1038/s41586-021-03197-9.
16. Metzger, M.B., and Weissman, A.M. (2010). Working on a chain: E3s ganging up for ubiquitylation. Nat Cell Biol *12*, 1124-1126. https://doi.org/10.1038/ncb1210-1124.
17. Yu, Y., Zheng, Q., Erramilli, S.K., Pan, M., Park, S., Xie, Y., Li, J., Fei, J., Kossiakoff, A.A., Liu, L., and Zhao, M. (2021). K29-linked ubiquitin signaling regulates proteotoxic stress response and cell cycle. Nat Chem Biol *17*, 896-905. https://doi.org/10.1038/s41589-021-00823-5.
18. Meyer, J.G., Kim, S., Maltby, D.A., Ghassemian, M., Bandeira, N., and Komives, E.A. (2014). Expanding proteome coverage with orthogonal-specificity alpha-lytic proteases. Mol Cell Proteomics *13*, 823-835. https://doi.org/10.1074/mcp.M113.034710.
19. Swatek, K.N., Usher, J.L., Kueck, A.F., Gladkova, C., Mevissen, T.E.T., Pruneda, J.N., Skern, T., and Komander, D. (2019). Insights into ubiquitin chain architecture using Ub-clipping. Nature *572*, 533-537. https://doi.org/10.1038/s41586-019-1482-y.
20. Zheng, Q., Wang, T., Chu, G.C., Zuo, C., Zhao, R., Sui, X., Ye, L., Yu, Y., Chen, J., Wu, X., et al. (2020). An E1-Catalyzed Chemoenzymatic Strategy to Isopeptide-N-Ethylated Deubiquitylase-Resistant Ubiquitin Probes. Angew Chem Int Ed Engl *59*, 13496-13501. https://doi.org/10.1002/anie.202002974.
21. Zheng, Q., Wang, T., Mao, J., Chu, G., Liang, L., Jing, Y., Zuo, C., Yu, Y., Hu, H., and Pan, M. (2023). A bifunctional molecule-assisted synthesis

of mimics for use in probing the ubiquitination system. Nat Protoc *18*, 530-554. https://doi.org/10.1038/s41596-022-00761-z.

22. Ai, H., Tong, Z., Deng, Z., Tian, J., Zhang, L., Sun, M., Du, Y., Xu, Z., Shi, Q., Liang, L., et al. (2023). Synthetic E2-Ub-nucleosome conjugates for studying nucleosome ubiquitination. Chem. https://doi.org/10.1016/j.chempr.2023.01.012.

23. Xie, Y., and Varshavsky, A. (2002). UFD4 lacking the proteasome-binding region catalyses ubiquitination but is impaired in proteolysis. Nat Cell Biol *4*, 1003-1007. https://doi.org/10.1038/ncb889.

24. Békés, M., van der Heden van Noort, G.J., Ekkebus, R., Ovaa, H., Huang, T.T., and Lima, C.D. (2016). Recognition of Lys48-Linked Di-ubiquitin and Deubiquitinating Activities of the SARS Coronavirus Papain-like Protease. Mol Cell *62*, 572-585. https://doi.org/10.1016/j.molcel.2016.04.016.

25. Kristariyanto, Y.A., Abdul Rehman, S.A., Weidlich, S., Knebel, A., and Kulathu, Y. (2017). A single MIU motif of MINDY-1 recognizes K48-linked polyubiquitin chains. EMBO Rep *18*, 392-402. https://doi.org/10.15252/embr.201643205.

26. Liu, Z., Dong, X., Yi, H.W., Yang, J., Gong, Z., Wang, Y., Liu, K., Zhang, W.P., and Tang, C. (2019). Structural basis for the recognition of K48-linked Ub chain by proteasomal receptor Rpn13. Cell Discov *5*, 19. https://doi.org/10.1038/s41421-019-0089-7.

27. Abdul Rehman, S.A., Armstrong, L.A., Lange, S.M., Kristariyanto, Y.A., Gräwert, T.W., Knebel, A., Svergun, D.I., and Kulathu, Y. (2021). Mechanism of activation and regulation of deubiquitinase activity in MINDY1 and MINDY2. Mol Cell *81*, 4176-4190.e4176. https://doi.org/10.1016/j.molcel.2021.08.024.

28. Maspero, E., Valentini, E., Mari, S., Cecatiello, V., Soffientini, P., Pasqualato, S., and Polo, S. (2013). Structure of a ubiquitin-loaded HECT ligase reveals the molecular basis for catalytic priming. Nat Struct Mol Biol *20*, 696-701. https://doi.org/10.1038/nsmb.2566.

29. Kamadurai, H.B., Qiu, Y., Deng, A., Harrison, J.S., Macdonald, C., Actis, M., Rodrigues, P., Miller, D.J., Souphron, J., Lewis, S.M., et al. (2013). Mechanism of ubiquitin ligation and lysine prioritization by a HECT E3. Elife *2*, e00828. https://doi.org/10.7554/eLife.00828.

30. Kamadurai, H.B., Souphron, J., Scott, D.C., Duda, D.M., Miller, D.J., Stringer, D., Piper, R.C., and Schulman, B.A. (2009). Insights into ubiquitin transfer cascades from a structure of a UbcH5B approximately ubiquitin-HECT(NEDD4L) complex. Mol Cell *36*, 1095-1102. https://doi.org/10.1016/j.molcel.2009.11.010.

31. Huang, L., Kinnucan, E., Wang, G., Beaudenon, S., Howley, P.M., Huibregtse, J.M., and Pavletich, N.P. (1999). Structure of an

E6AP-UbcH7 complex: insights into ubiquitination by the E2-E3 enzyme cascade. Science *286*, 1321-1326. https://doi.org/10.1126/science.286.5443.1321.

32. Kaiho-Soma, A., Akizuki, Y., Igarashi, K., Endo, A., Shoda, T., Kawase, Y., Demizu, Y., Naito, M., Saeki, Y., Tanaka, K., and Ohtake, F. (2021). TRIP12 promotes small-molecule-induced degradation through K29/K48-branched ubiquitin chains. Mol Cell *81*, 1411-1424.e1417. https://doi.org/10.1016/j.molcel.2021.01.023.

33. Cotton, T.R., Cobbold, S.A., Bernardini, J.P., Richardson, L.W., Wang, X.S., and Lechtenberg, B.C. (2022). Structural basis of K63-ubiquitin chain formation by the Gordon-Holmes syndrome RBR E3 ubiquitin ligase RNF216. Mol Cell *82*, 598-615.e598. https://doi.org/10.1016/j.molcel.2021.12.005.

34. Stieglitz, B., Rana, R.R., Koliopoulos, M.G., Morris-Davies, A.C., Schaeffer, V., Christodoulou, E., Howell, S., Brown, N.R., Dikic, I., and Rittinger, K. (2013). Structural basis for ligase-specific conjugation of linear ubiquitin chains by HOIP. Nature *503*, 422-426. https://doi.org/10.1038/nature12638.

35. Ohtake, F., Saeki, Y., Ishido, S., Kanno, J., and Tanaka, K. (2016). The K48-K63 Branched Ubiquitin Chain Regulates NF-κB Signaling. Mol Cell *64*, 251-266. https://doi.org/10.1016/j.molcel.2016.09.014.

36. Tang, S., Liang, L.J., Si, Y.Y., Gao, S., Wang, J.X., Liang, J., Mei, Z., Zheng, J.S., and Liu, L. (2017). Practical Chemical Synthesis of Atypical Ubiquitin Chains by Using an Isopeptide-Linked Ub Isomer. Angew Chem Int Ed Engl *56*, 13333-13337. https://doi.org/10.1002/anie.201708067.

37. Li, Y.T., Liang, J., Li, J.B., Fang, G.M., Huang, Y., and Liu, L. (2014). New semi-synthesis of ubiquitin C-terminal conjugate with 7-amino-4-methylcoumarin. J Pept Sci *20*, 102-107. https://doi.org/10.1002/psc.2568.

38. Haakonsen, D.L., and Rape, M. (2019). Branching Out: Improved Signaling by Heterotypic Ubiquitin Chains. Trends Cell Biol *29*, 704-716. 10.1016/j.tcb.2019.06.003.

39. Wertz, I.E., Newton, K., Seshasayee, D., Kusam, S., Lam, C., Zhang, J., Popovych, N., Helgason, E., Schoeffler, A., Jeet, S., et al. (2015). Phosphorylation and linear ubiquitin direct A20 inhibition of inflammation. Nature *528*, 370-375. https://doi.org/10.1038/nature16165.

40. Yau, R.G., Doerner, K., Castellanos, E.R., Haakonsen, D.L., Werner, A., Wang, N., Yang, X.W., Martinez-Martin, N., Matsumoto, M.L., Dixit, V.M., and Rape, M. (2017). Assembly and Function of Heterotypic Ubiquitin Chains in Cell-Cycle and Protein Quality Control. Cell *171*,

918-933.e920. https://doi.org/10.1016/j.cell.2017.09.040.

41. Chen, Y.H., Huang, T.Y., Lin, Y.T., Lin, S.Y., Li, W.H., Hsiao, H.J., Yan, R.L., Tang, H.W., Shen, Z.Q., Chen, G.C., et al. (2021). VPS34 K29/K48 branched ubiquitination governed by UBE3C and TRABID regulates autophagy, proteostasis and liver metabolism. Nat Commun *12*, 1322. https://doi.org/10.1038/s41467-021-21715-1.

42. Zheng, S.Q., Palovcak, E., Armache, J.P., Verba, K.A., Cheng, Y., and Agard, D.A. (2017). MotionCor2: anisotropic correction of beam-induced motion for improved cryo-electron microscopy. Nat Methods *14*, 331-332. https://doi.org/10.1038/nmeth.4193.

43. Mindell, J.A., and Grigorieff, N. (2003). Accurate determination of local defocus and specimen tilt in electron microscopy. J Struct Biol *142*, 334-347. https://doi.org/10.1016/s1047-8477(03)00069-8.

44. Zivanov, J., Nakane, T., Forsberg, B.O., Kimanius, D., Hagen, W.J., Lindahl, E., and Scheres, S.H. (2018). New tools for automated high-resolution cryo-EM structure determination in RELION-3. Elife *7*. https://doi.org/10.7554/eLife.42166.

45. Pettersen, E.F., Goddard, T.D., Huang, C.C., Meng, E.C., Couch, G.S., Croll, T.I., Morris, J.H., and Ferrin, T.E. (2021). UCSF ChimeraX: Structure visualization for researchers, educators, and developers. Protein Sci *30*, 70-82. https://doi.org/10.1002/pro.3943.

46. Emsley, P., and Cowtan, K. (2004). Coot: model-building tools for molecular graphics. Acta Crystallogr D Biol Crystallogr *60*, 2126-2132. https://doi.org/10.1107/s0907444904019158.

47. Adams, P.D., Afonine, P.V., Bunkóczi, G., Chen, V.B., Davis, I.W., Echols, N., Headd, J.J., Hung, L.W., Kapral, G.J., Grosse-Kunstleve, R.W., et al. (2010). PHENIX: a comprehensive Python-based system for macromolecular structure solution. Acta Crystallogr D Biol Crystallogr *66*, 213-221. https://doi.org/10.1107/s0907444909052925.

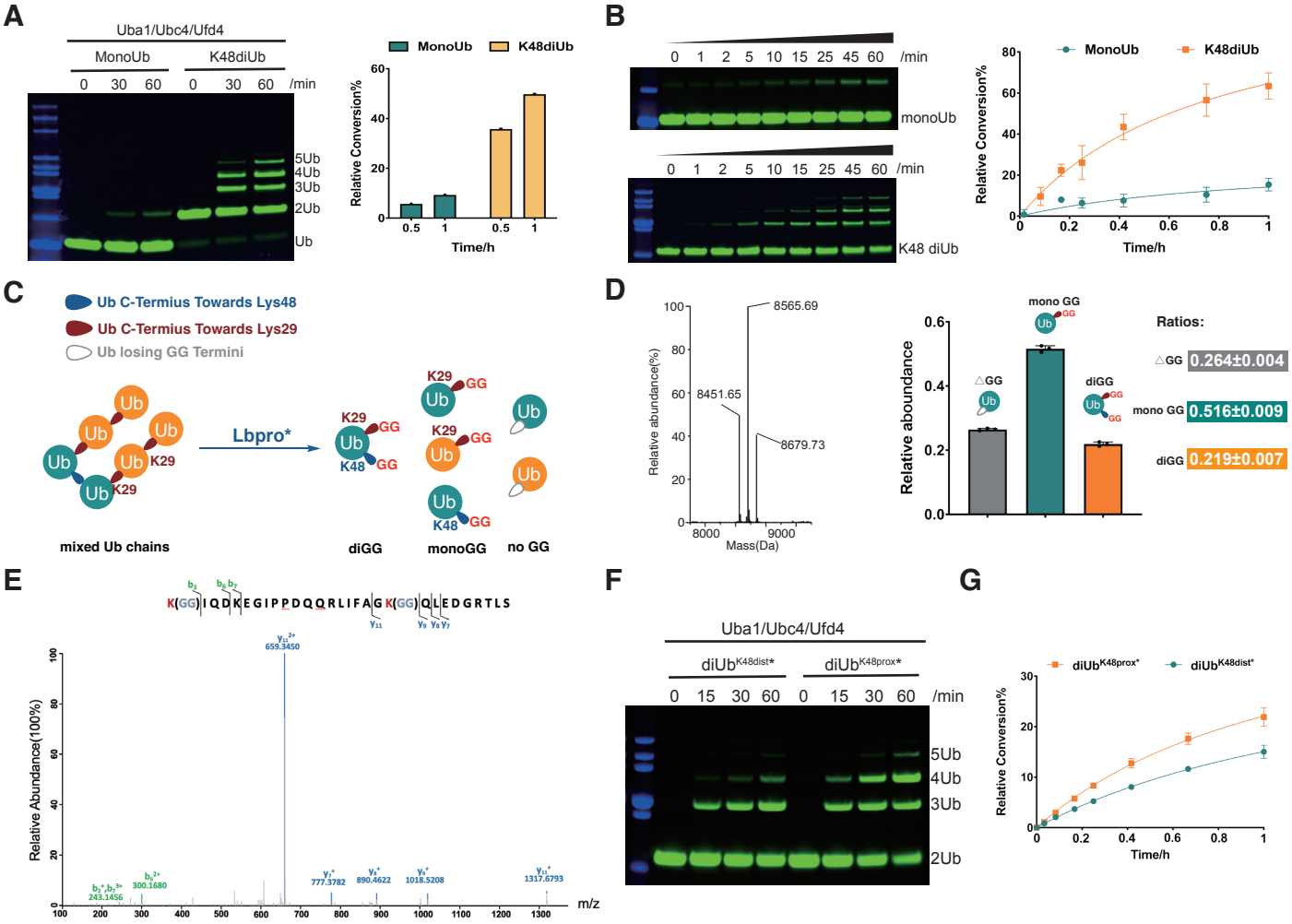

Figure 1. Ufd4 prefers to ubiquitinate on the proximal Lys29 of K48-linked diUb

(**A**) Ufd4-dependent in vitro ubiquitination on fluorescent MonoUb and K48-linked diUb. Gel images and columns of relative conversions (%).

(**B**) Ubiquitination assays described in (**A**) and sampling at indicated time points (0, 1, 2, 5, 10, 15, 25, 45, 60, /min), gel images and curves of relative conversions (%).

(**C**) Schematic representation of the identification flow of Ub linkage generated by Ufd4 on K48-linked Ub chains. The blue symbols represent peptide bond between Lys48 and Ub C-terminal, the red symbols represent peptide bond between Lys29 and Ub C-terminal, the grey symbols represent Ub C-terminals.

(**D**) Intact MS analysis of Lb^{pro*} treated in vitro ubiquitination reactions,and the spectra were deconvoluted. The mean value is shown from independent biological replicates (n = 3). Deconvoluted spectra (left), quantification of the relative abundance of each ubiquitin species (right).

(**E**) Identification of K29-K48 branched ubiquitin chains. The MS/MS spectrum corresponding to the signature peptide derived from K29-K48 branched linkages (aa 29–57, GlyGly modified at K29 and K48) was obtained.

(**F** and **G**) Ufd4-dependent in vitro ubiquitination on fluorescent K48-linked diUb with lysine to cysteine mutation at the proximal ($diUb^{K48prox*}$) or distal ($diUb^{K48dist*}$) Lys29 sites (**F**), and curves (**G**) of relative conversions (%) at indicated time points (As in **B**).Gel images and curves in **B** and **G** are representatives of independent biological replicates (n = 3).

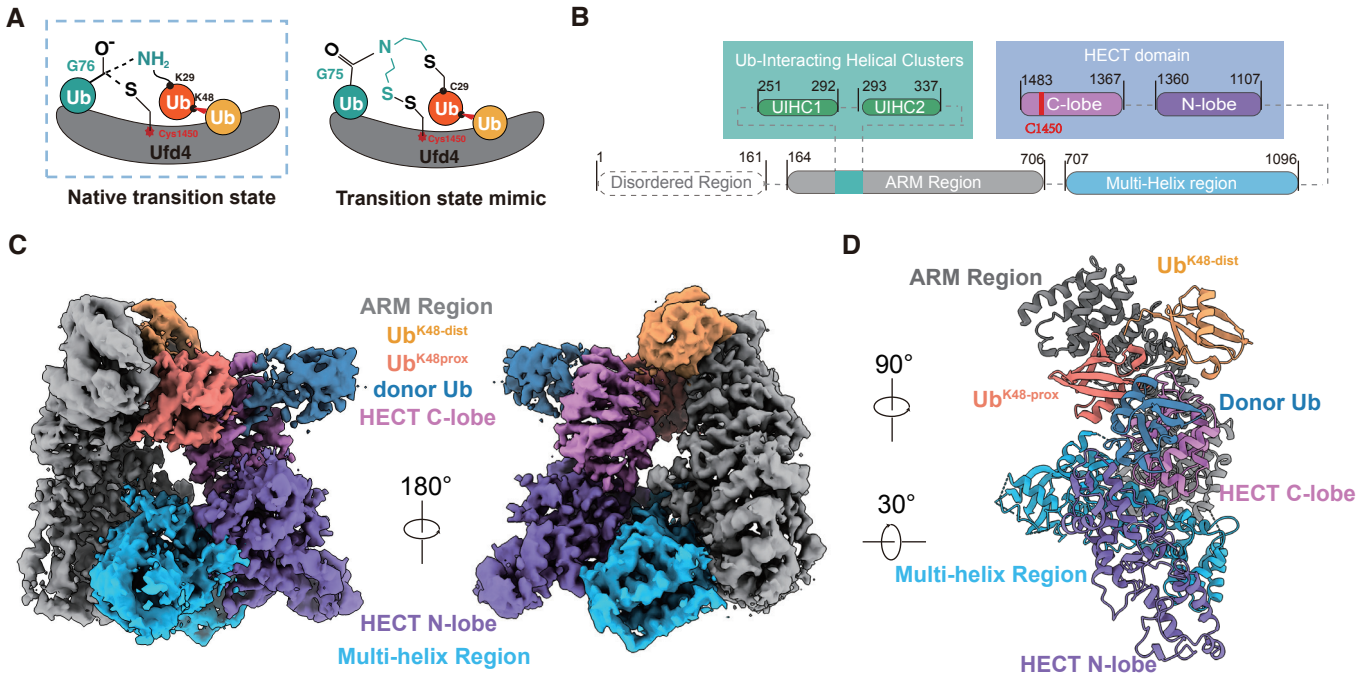

Figure. 2. Overall structure of Ufd4 in complex with triUb$^{K29/K48}$

(**A**) Schematic diagram of the native state vs. the transition state of the ubiquitination process. The side chain of a Lys residue on K48-linked diUb attacks the thioester bond of Ufd4–Ub. An intermediate structure design is shown in the inset to mimic the transition state of Ufd4-mediated Ub assembly.

(**B**) Structural domain diagram of Ufd4 with indicated residue boundaries. The dotted lines indicates unresolved N-terminus regions, the turquoise box represents the Ub binding domains, the dusty blue box indicates the HECT domain and the red line represents the active Cys1450.

(**C** and **D**) Cryo-EM density (**C**) and structural model (**D**) of the Ufd4-triUb$^{K29/K48}$ complex.

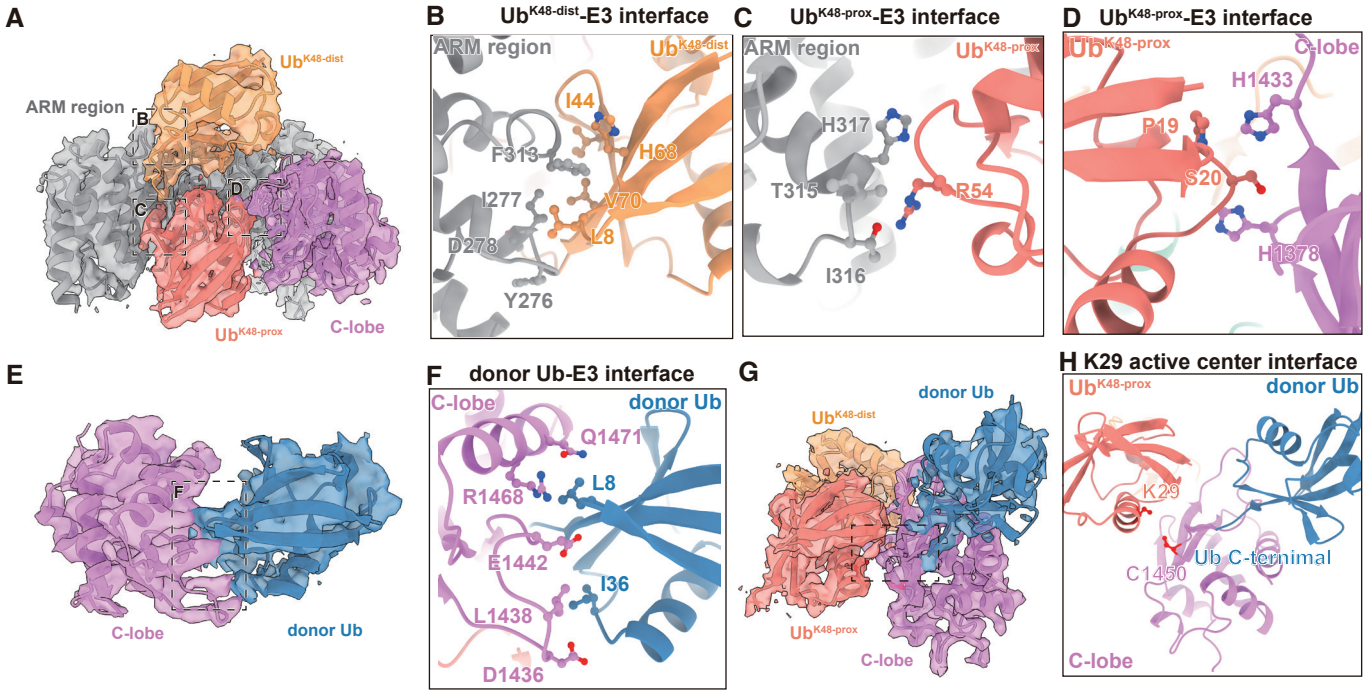

Figure. 3. Analysis of the interactions between Ufd4 and triUb$^{K29/K48}$

(**A**) Cryo-EM density of the ARM region and the HECT C-lobe with K48-linked diUb, dashed regions correspond to interfaces between Ufd4 and Ub$^{K48\text{-}dist}$, Ufd4 and Ub$^{K48\text{-}prox}$.

(**B**-**D**) Molecular interactions between the ARM region and Ub$^{K48\text{-}dist}$ (**B**), the ARM region and Ub$^{K48\text{-}prox}$ (**C**), the HECT C-lobe and Ub$^{K48\text{-}prox}$ (**D**).

(**E**) Cryo-EM density of the HECT C-lobe with donor Ub, dashed regions correspond to the noncovalent interfaces between the HECT C-lobe and donor Ub.

(**F**) Molecular interactions between the HECT C-lobe and donor Ub.

(**G** and **H**) Cryo-EM density of the HECT C-lobe with triUbK29/K48 (**G**), dashed regions correspond to interfaces between HECT C-lobe Cys1450, Lys29 of Ub$^{K48\text{-}prox}$ and C-terminal of donor Ub (**H**).

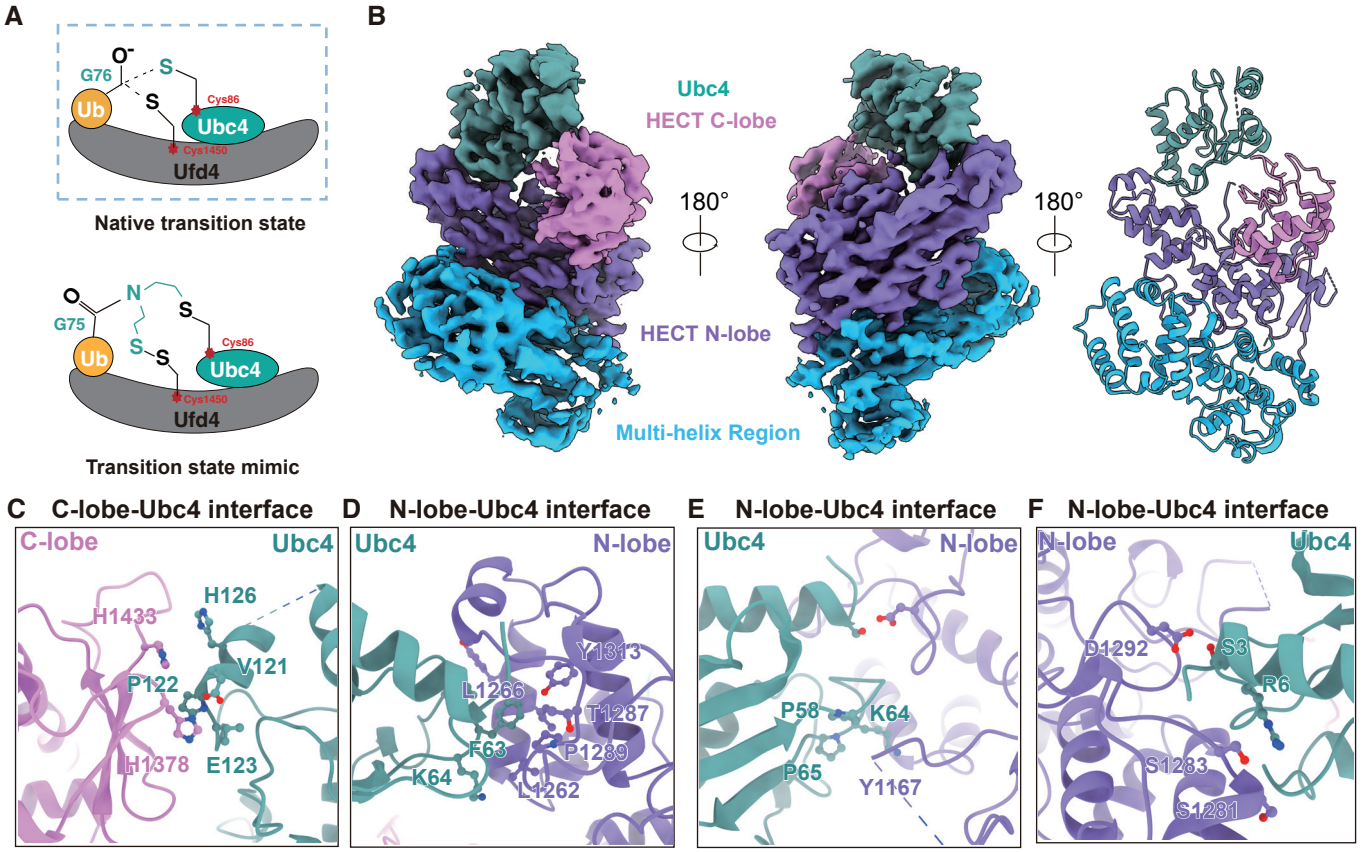

Figure. 4. The structure of Ufd4 in complex with Ubc4-Ub.
(**A**) Schematic diagram of the native state vs. the transition state of the transthiolation process. The side chain of a Cys residue on Ufd4 attacks the thioester bond of Ubc4–Ub. An intermediate structure design is shown in the inset to mimic the transition state of Ufd4-mediated transthiolation process.
(**B**) Cryo-EM density and structural model of the Ufd4$^{\triangle ARM}$-Ubc4 complex.
(**C**-**F**) Molecular interactions between the HECT C-lobe and Ubc4 (**C**), the HECT N-lobe and Ubc4 (**D**-**F**).

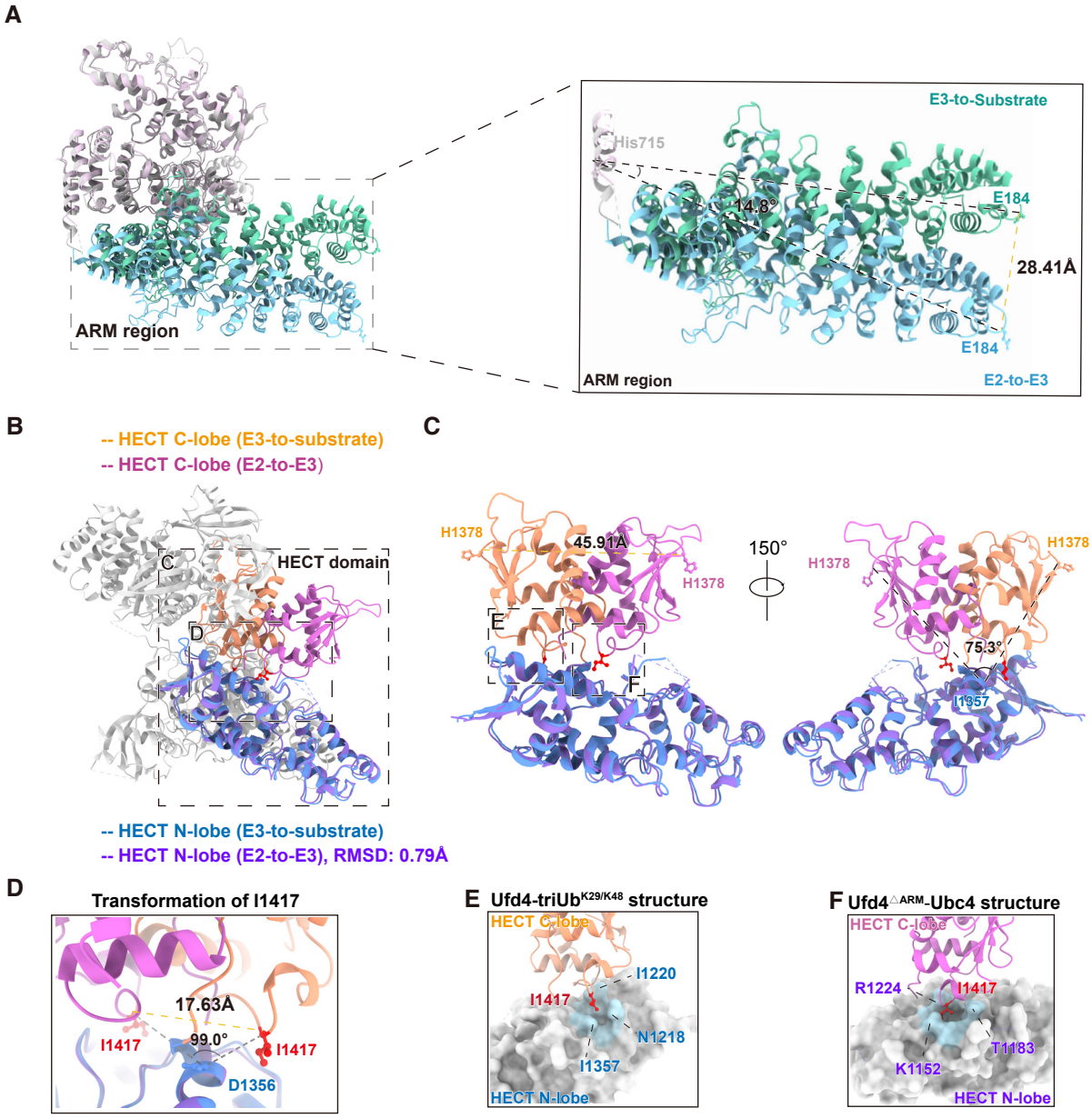

Figure. 5. Transition from transthiolation to K29-linked Ub assembly.
(**A**) Structural alignment of Ufd4-Ubc4 and Ufd4-triUb$^{K29/K48}$ structures. The ARM region in the Ufd4-Ubc4 structure is colored sky blue, and in Ufd4-triUb$^{K29/K48}$ structure is colored green. Root-mean-square deviation (RMSD) of backbone atoms is indicated. Distance between residue Glu184 α carbon and angle of Glu184 relative to His715 are shown.
(**B**-**D**) Structural alignment of the HECT domain in Ufd4$^{\triangle ARM}$-Ubc4 and Ufd4-triUb$^{K29/K48}$ structures (**B**). The HECT C-lobe in the Ufd4$^{\triangle ARM}$-Ubc4 structure is colored pink, and in Ufd4-triUb$^{K29/K48}$ structure is colored orange. Root-mean-square deviation (RMSD) of backbone atoms are indicated; The distance between His1378 α carbon and angle of His1378 relative to Ile1357 are shown (**C**). The distance between Ile1417 and angle of Ile1417 relative to Asp1356 are shown (**D**).
(**E** and **F**) Molecular interactions between residue Ile1417 and the HECT N-lobe in Ufd4$^{\triangle ARM}$-Ubc4 (**E**) and in Ufd4-triUb$^{K29/K48}$ (**F**).

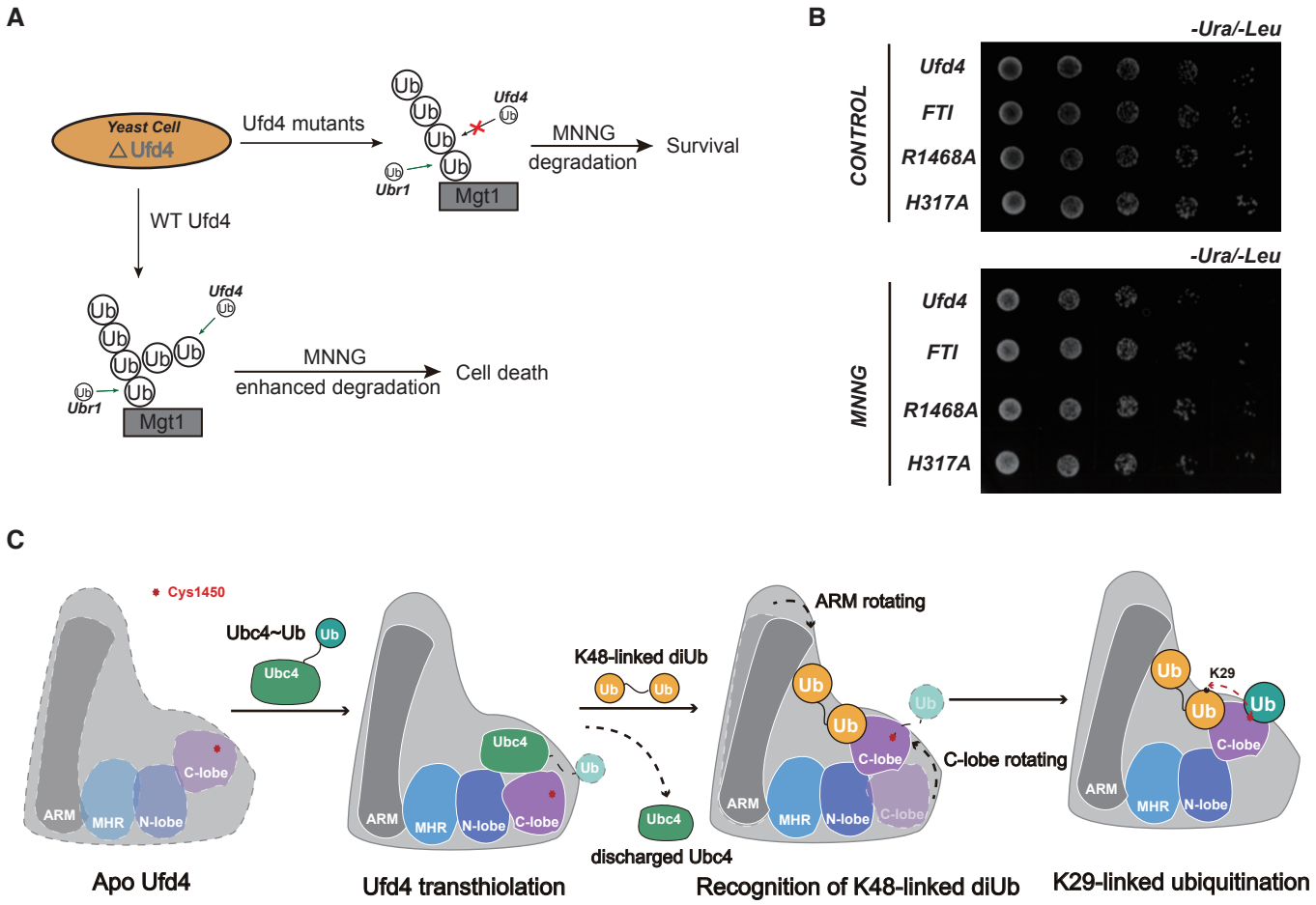

Figure.6. A model of Ufd4-mediated Ub assembly on K48-linked diUb

(**A**) The design of yeast growth assay. The yeast growth status is influenced by Mgt1 level. If wild-type Ufd4 is supplemented, Mgt1 will be rapidly polyubiquitinated and degraded which lead to cell death; Supplementation of Ufd4 mutants will slow down the polyubiquitination and promote cell survival.

(**B**) Yeast strains carrying wild-type Ufd4 or Ufd4 mutants (FTI, R1468A and H317A) were dropped on dextrose-containing (SD) plates with or without MNNG. The plates were incubated at 30 °C for 2 d.

(**C**) A cartoon representation of Ufd4-mediated ubiquitination beginning with transthiolation from Ubc4~Ub to K29-linked ubiquitination. The last three steps correspond to the transthiolation, conformational changes, K29-linked ubiquitination processes described in this study. The apo Ufd4 structure is based on AlphaFold (AF-P33202-F1) which is hypothetical.

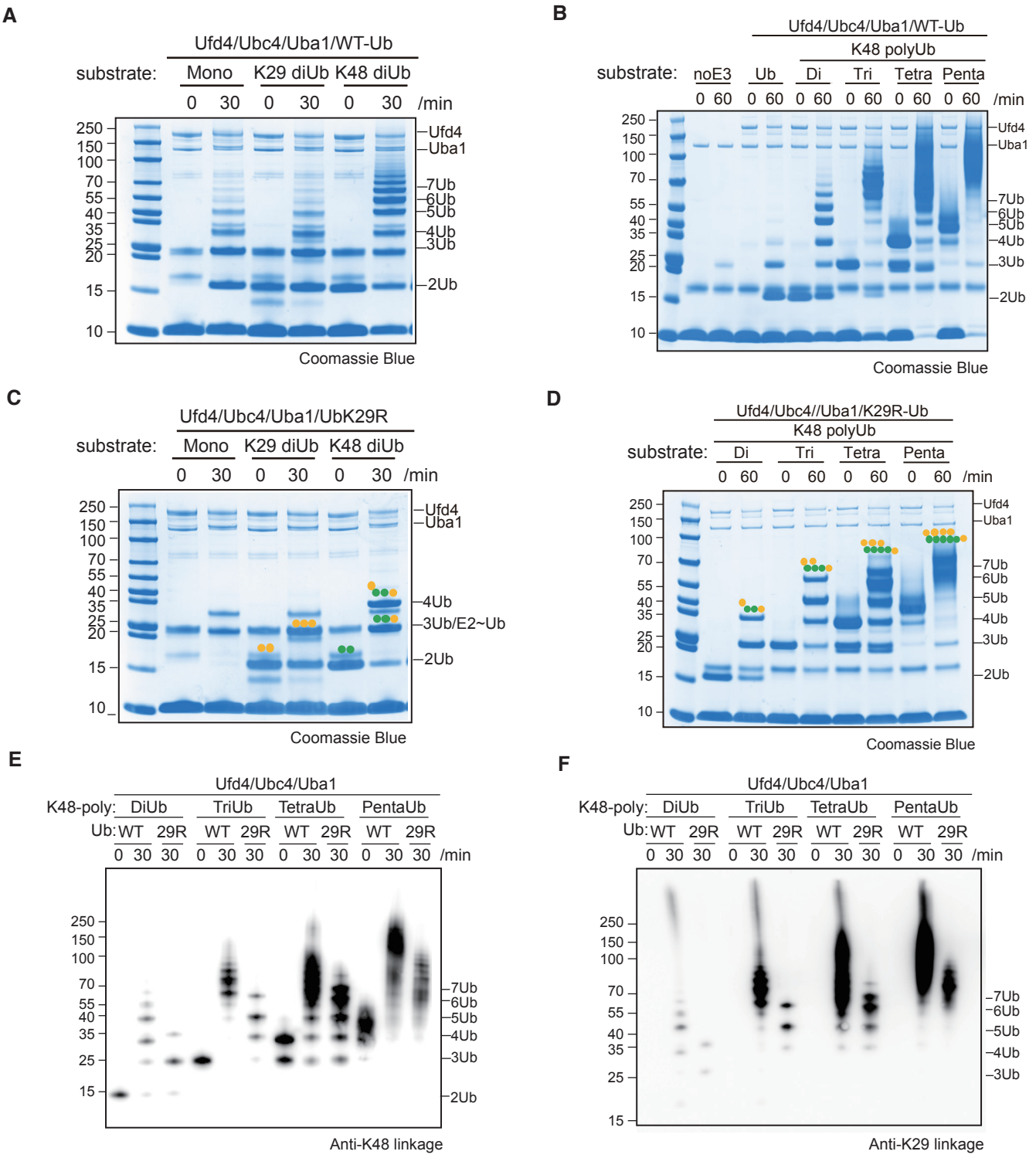

Figure S1: Ufd4 prefer to ubiquitinate on K48-linked chains, related to Figure1
(**A**) *In vitro* Ufd4-dependent ubiquitination assays on monoUb, K29- and K48-linked diUb.
(**B**) *In vitro* Ufd4-dependent ubiquitination assyas on different length of K48-linked Ub chains.
(**C** and **D**) As in (A), substitute wild-type Ub with Ub-K29R mutant (**C**); As in (**B**) substitute wild-type Ub with Ub-K29R mutant (**D**).
(**E** and **F**) Western blot Analysis using anti-K48 and anti-K29 antibodies as in (**C**) and (**D**).

A

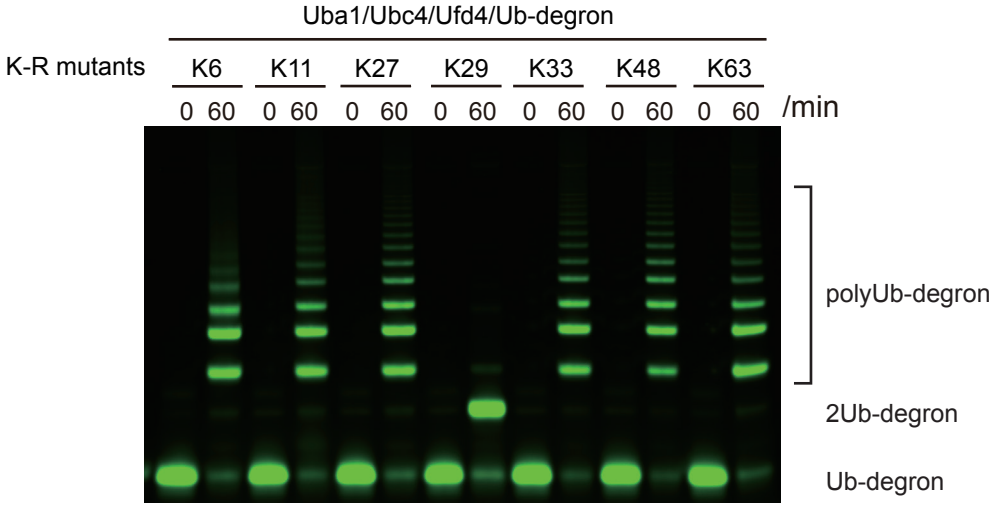

B

MS-MS result of polyUb using WT Ub, 93% of K29-linked ub chains

Linkage	Ubiquitin Sequence	#PSMs	Modifications	Area
K29	A**k**IQDKEGIPPDQQR	42	K2(GlyGly)	1.769E10
K29/K33	A**k**IQD**k**EGIPPDQQR	2	K2(GlyGly); K6(GlyGly)	2.781E7
K63	TLSDYNIQ**k**ESTLHLVLRLR	4	K9(GlyGly)	6.194E8
K63	TLSDYNIQ**k**ESTLHLVLR	1	K9(GlyGly)	3.322E8
K6	MQIFV**k**TLTGK	3	K6(GlyGly)	1.690E8
K11	TLTG**k**TITLEVEPSDTIENVK	1	K5(GlyGly)	1.658E8
K48	LIFAG**k**QLEDGR	6	K6(GlyGly)	1.063E8

Figure S2: Analysis of ubiquitin chain linkage generated by Ufd4,related to Figure1
(**A**) In vitro Ufd4-dependent ubiquitination on fluorescently labelled Ub-degron using seven Lys to Arg Ub mutations.
(**B**) Identification of Ub chain linkages generated by Ufd4 on wild-type Ub.

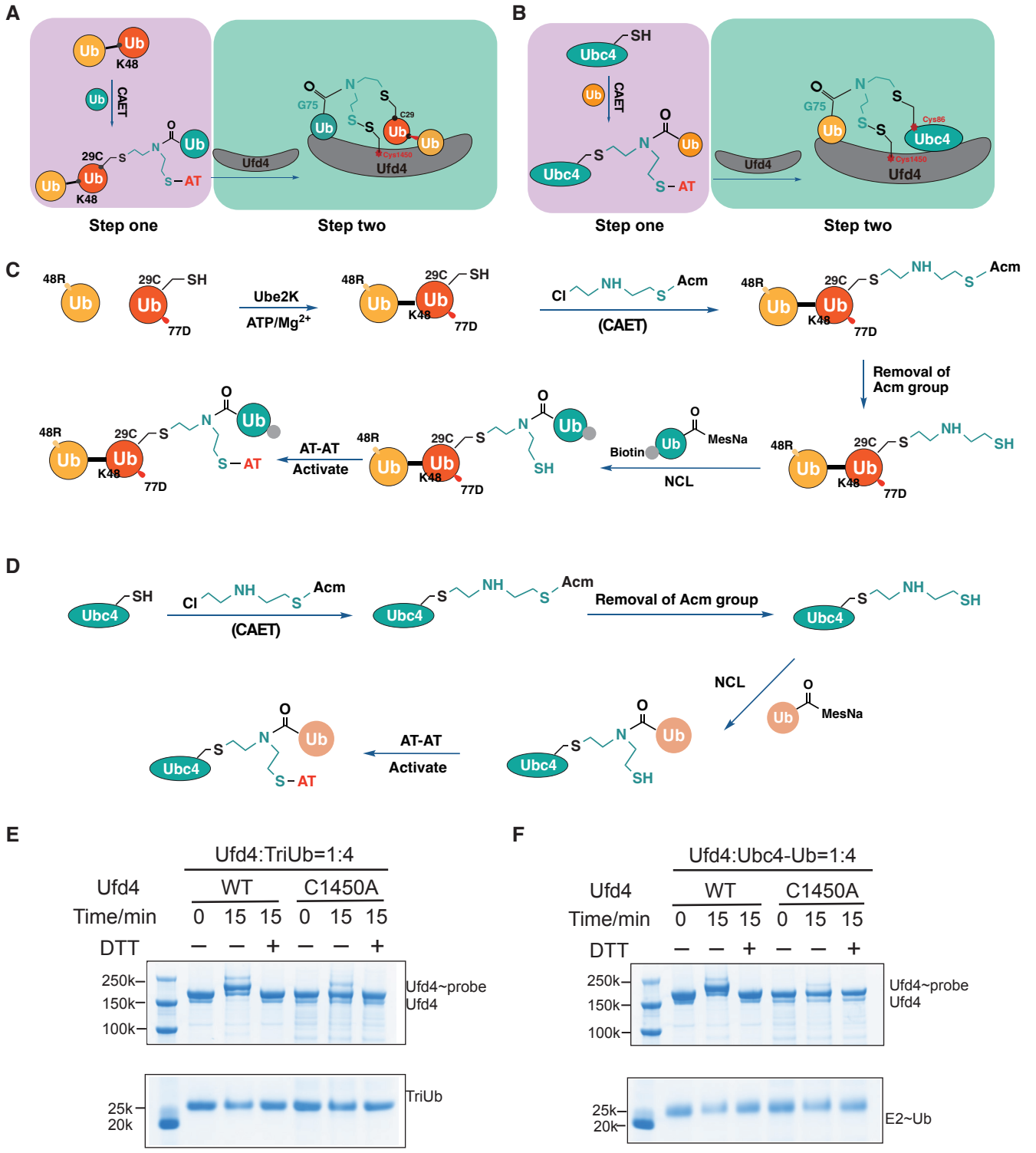

Figure S3: Synthesis and testing of activity-based probes related to Figure2
(**A** and **B**) Schematic of two-step complex assembly routes, Ufd4 in complex with triUb$^{K29/K48}$ (**A**) and Ufd4 in complex with Ubc4-Ub (**B**).
(**C**) A brief synthetic route of the intermediate structure mimicking the transition state of Ufd4 mediated ubiquitination at proximal Lys29 site of K48-linked diUb.
(**D**) A brief synthetic route of the intermediate structure mimicking the transition state of Ufd4 mediated transthiolation from Ubc4-Ub.
(**E** and **F**) In vitro crosslinking experiments between Ufd4 and triUb$^{K29/K48}$ (**E**) or ubc4-Ub (**F**), respectively.

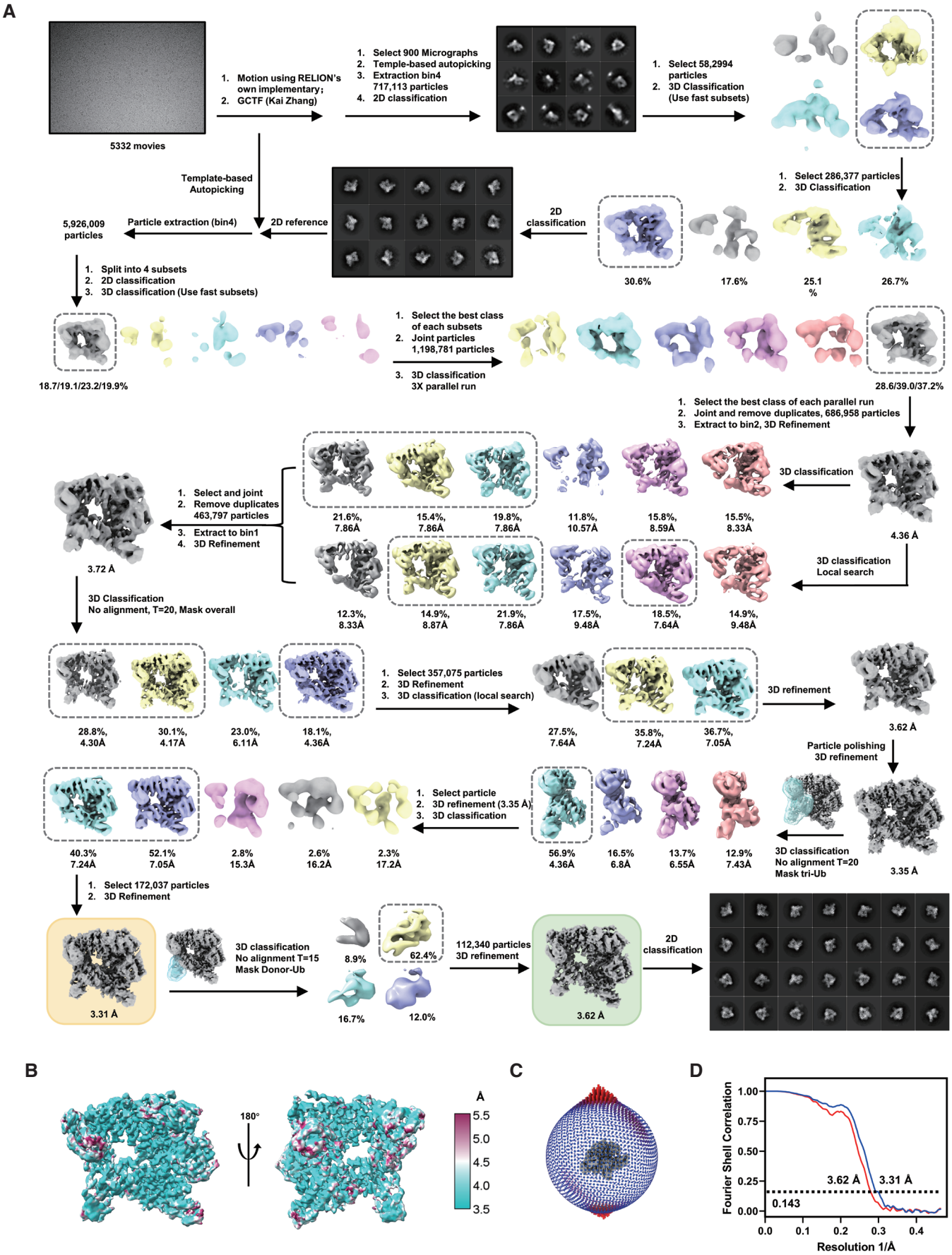

Figure S4: Single-particle cryo-EM analyses of Ufd4 with K29/K48-linked triUb, related to Figure2

(**A**) The workflow of Ufd4-triUb$^{K29/K48}$ complex cryo-EM data processing. The imageset was subjected to particle selection, 2D classification, and multiple rounds of 3D classification. Representative micrograph and 2D class averages are shown.

(**B**) The local resolution of the map calculated using Relion.

(**C**) The distribution of the Euler angles.

(**D**) Fourier shell correlation (FSC) curve of the masked map after Relion postprocessing. The resolution was determined by the FSC=0.143 criterion. The model vs. map FSC curve is also shown.

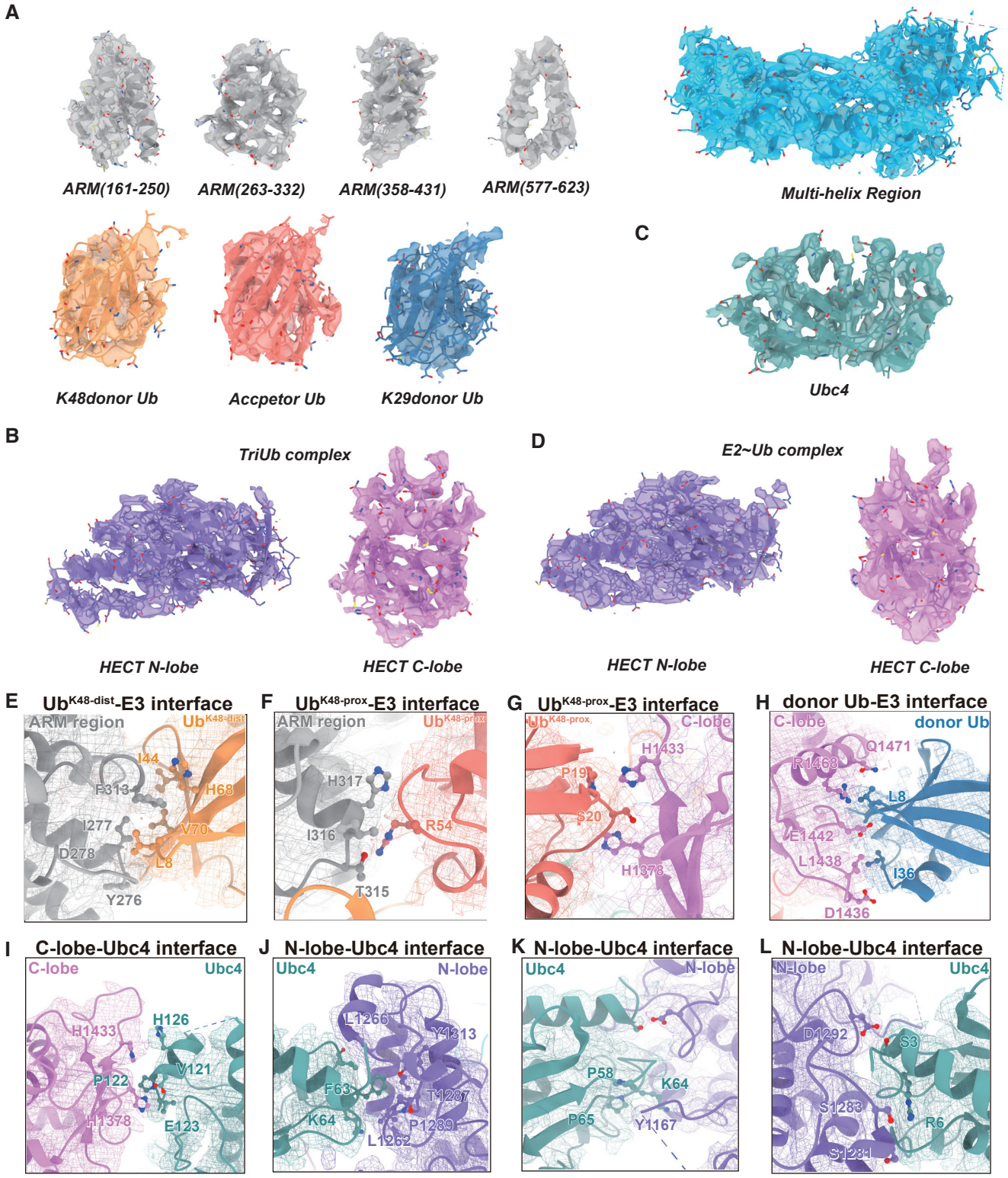

Figure S5. Cryo-EM density of the triUb$^{K29/K48}$ and E2-Ub complexes, related to Figure2-4

(**A**) Individual domains of Ufd4 in the Ufd4-triUb$^{K29/K48}$ complex.

(**B**-**D**) The HECT N-lobe and HECT C-lobe in the Ufd4-triUb$^{K29/K48}$ complex (**B**); The Ubc4 (**C**) and the HECT N-lobe and HECT C-lobe (**D**) in Ufd4-Ubc4-Ub complex.

(**E**-**H**) The ARM region and Ub$^{K48\text{-}dist}$ interfaces (**E**), the ARM region and Ub$^{K48\text{-}prox}$ interfaces (**F**), the HECT C-lobe and Ub$^{K48\text{-}prox}$ interfaces (**G**), the HECT C-lobe and donor Ub interfaces (**H**) in Ufd4-triUb$^{K29/K48}$ complex.

(**I**-**J**) The HECT C-lobe and Ubc4 interfaces (**I**), the HECT N-lobe and Ubc4 interfaces (**J**-**L**) in Ufd4-Ubc4-Ub complex.

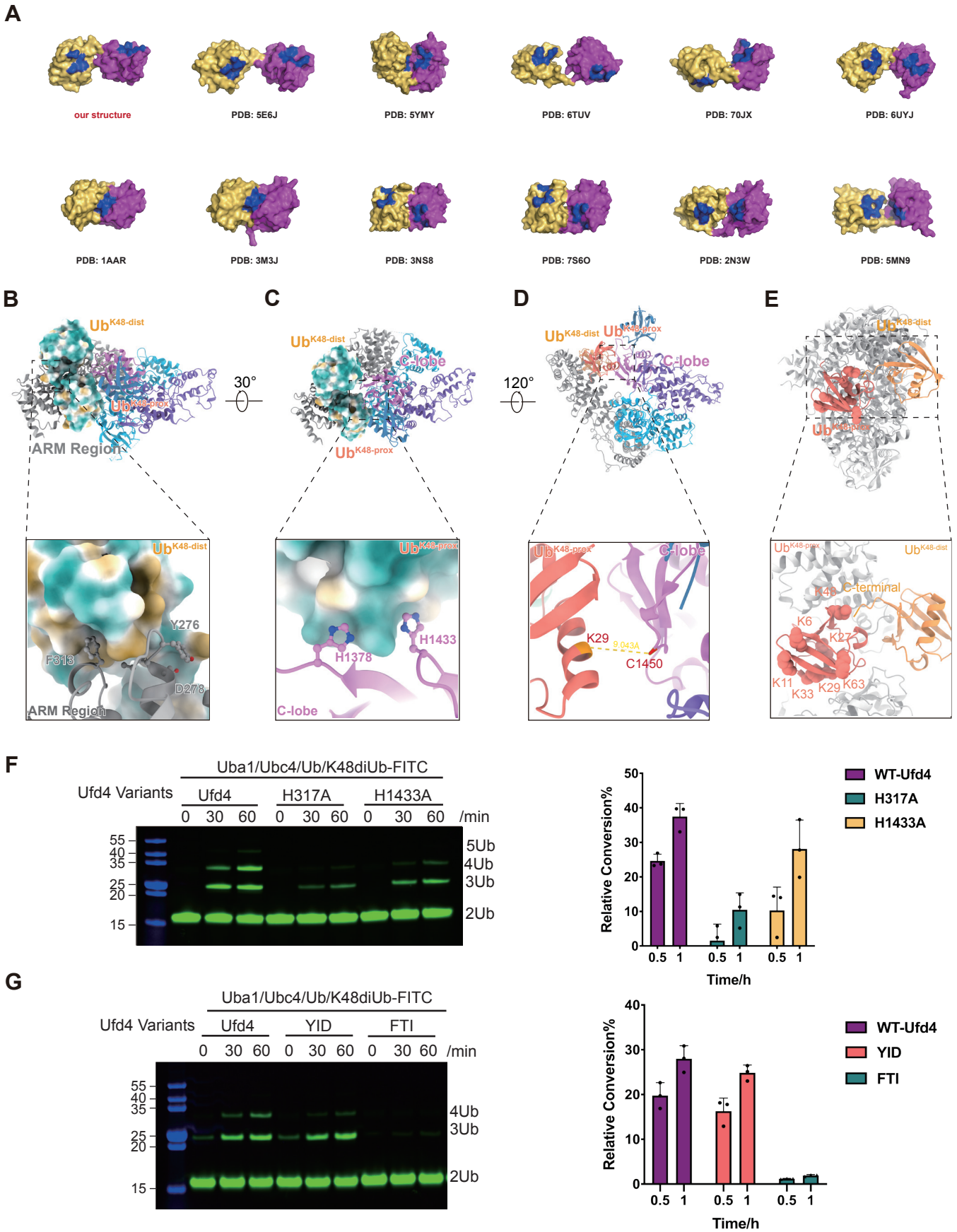

Figure S6: Analyses of the interactions between Ufd4 and K48diUb, related to Figure3

(**A**) Comparison of different K48-linked diUb structures shown in surface representation with distal ubiquitin shown in yellow proximal ubiquitin shown in magenta and the I44 patches highlighted in blue.

(**B**) The hydrophobic surface between residue Phe313 and $Ub^{K48\text{-}dist}$.

(**C**) The hydrophilic surface between residues His1378, His1433 and $Ub^{K48\text{-}prox}$. (**D**) The distance between $Ub^{K48\text{-}prox}$ residue Lys29 and the HECT C-lobe active center residue Cys1450.

(**E**) The linkage between Lys48 of $Ub^{K48\text{-}prox}$ and C-terminal of $Ub^{K48\text{-}dist}$.

(**F-G**) In vitro Ufd4-dependent ubiquitination assays. Mutations of H317A, H1433A (**F**), YID (Y276A/I277A/D278A), FTI (F313A/T315A/I316A) (**G**) are tested, and curves of relative conversions (%) are shown on the left side. Gel images and curves in **F** and **G** are representative of independent biological replicates (n = 3).

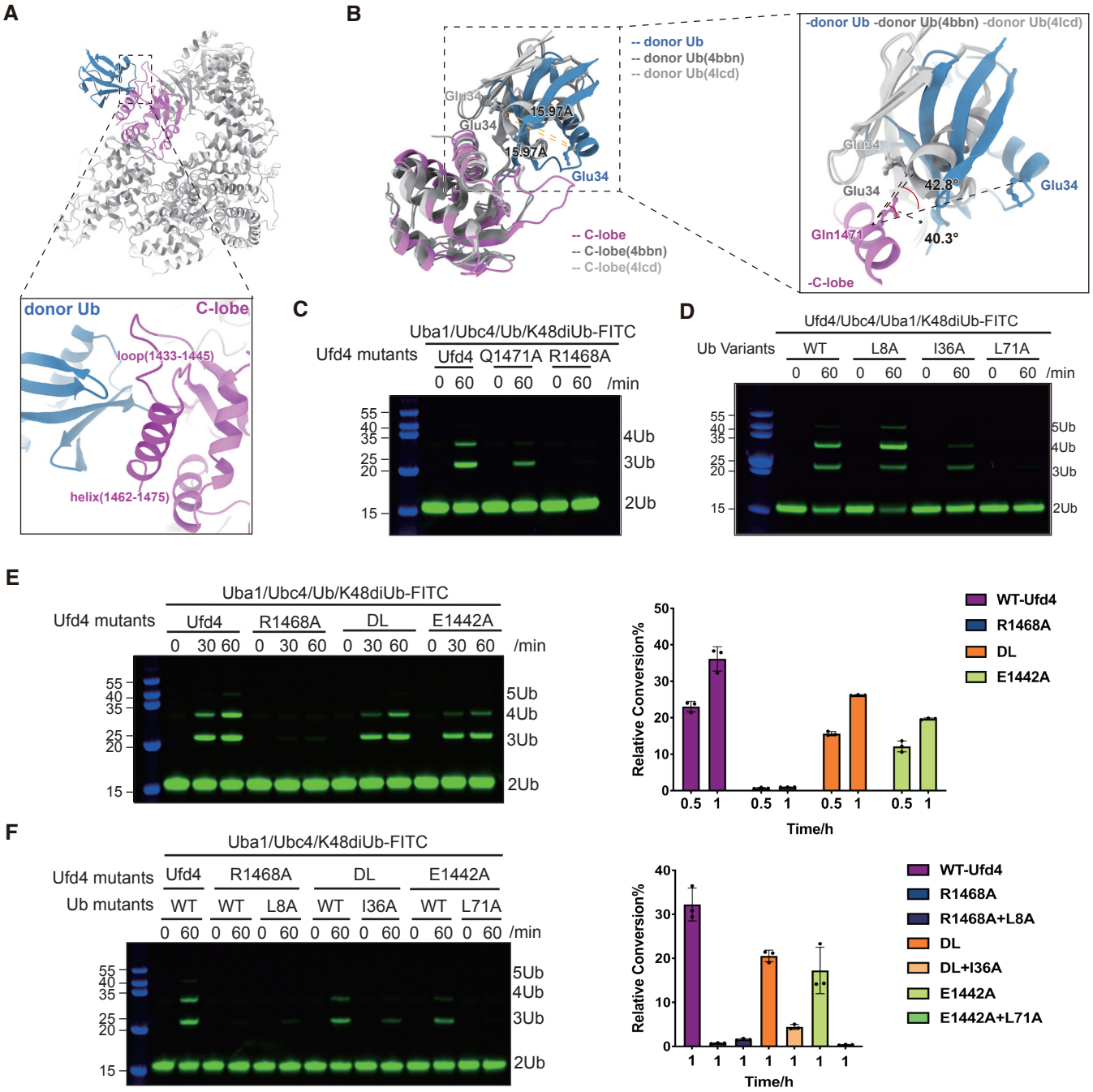

Figure S7: Analyses of the interactions between Ufd4 and K29 donor Ub, related to Figure3

(**A**) A close-up view of the interface between the HECT C-lobe and donor Ub.

(**B**) Structure alignment of HECT C-lobe and donor Ub determined in this study with Ub-loaded HECT ligase structure (4bbn) and HECT E3 Ub-substrate complex structure (4lcd). Root-mean-square deviation (RMSD) of backbone atoms are indicated.

(**C**-**F**) In vitro Ufd4-dependent ubiquitination assays. Mutations of Ufd4 R1468A, Q1471A (**C**), DL (D1436A/L1438A), E1442A (**E**) and mutations of donor Ub L8A, I36A, L71A (**D**), and simultaneous mutations of Ufd4 and donor Ub (**F**) are tested. Columns of relative conversions (%) are shown on the left. Gel images and columns in **C**, **E** and **F** are representative of independent biological replicates (n = 3).

.

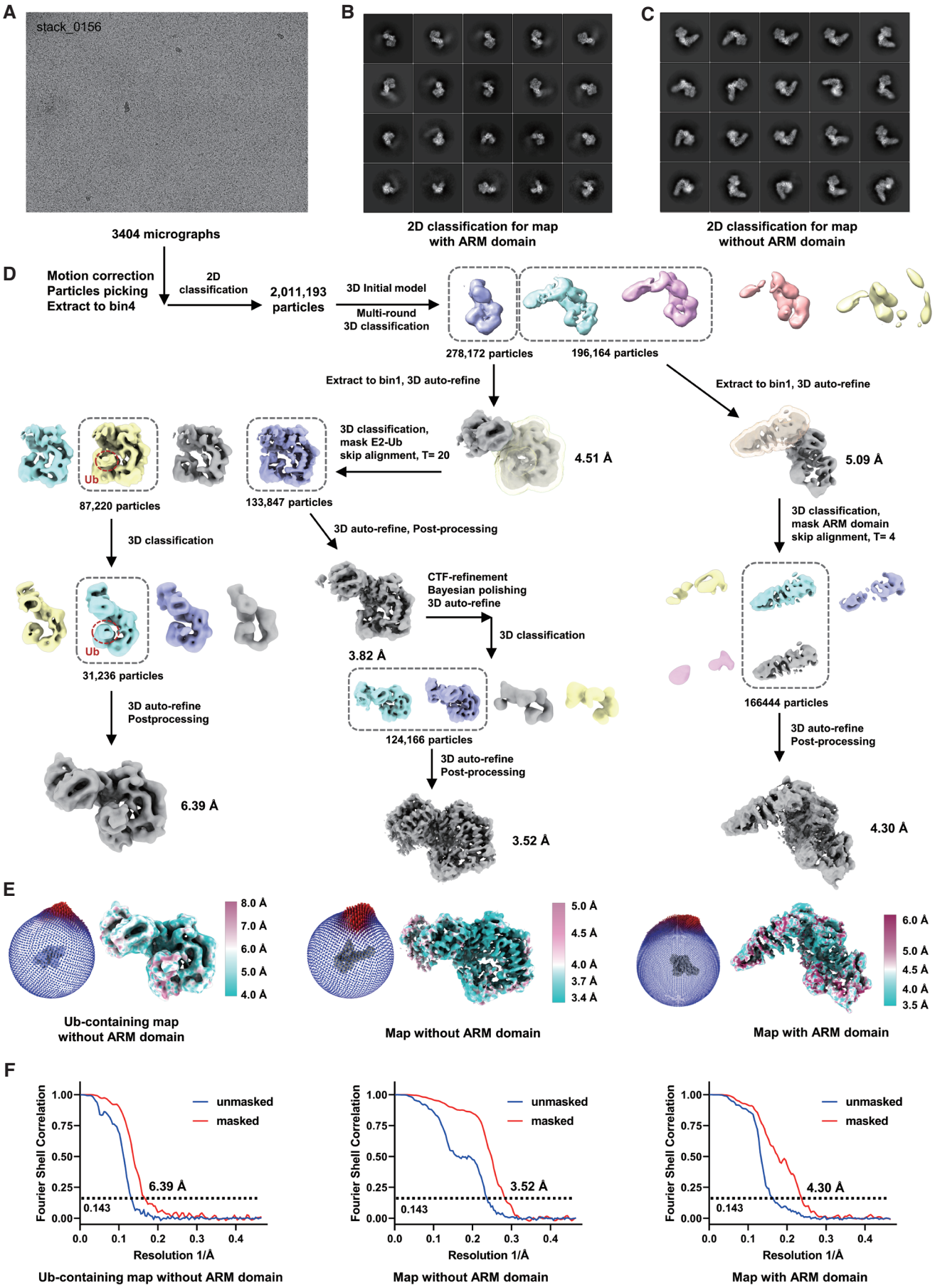

Figure S8: Single-particle cryo-EM analyses of Ufd4 with Ubc4~Ub, related to Figure4

(**A**-**C**) The workflow of Ufd4-Ubc4-Ub complex cryo-EM data processing. The imageset of was subjected to particle selection, 2D classification, and multiple rounds of 3D classification. Representative micrograph and 2D classes averages are shown.

(**D** and **E**) The distribution of the Euler angles (**D**) and FSC curves (**E**) of the masked maps after Relion postprocessing.

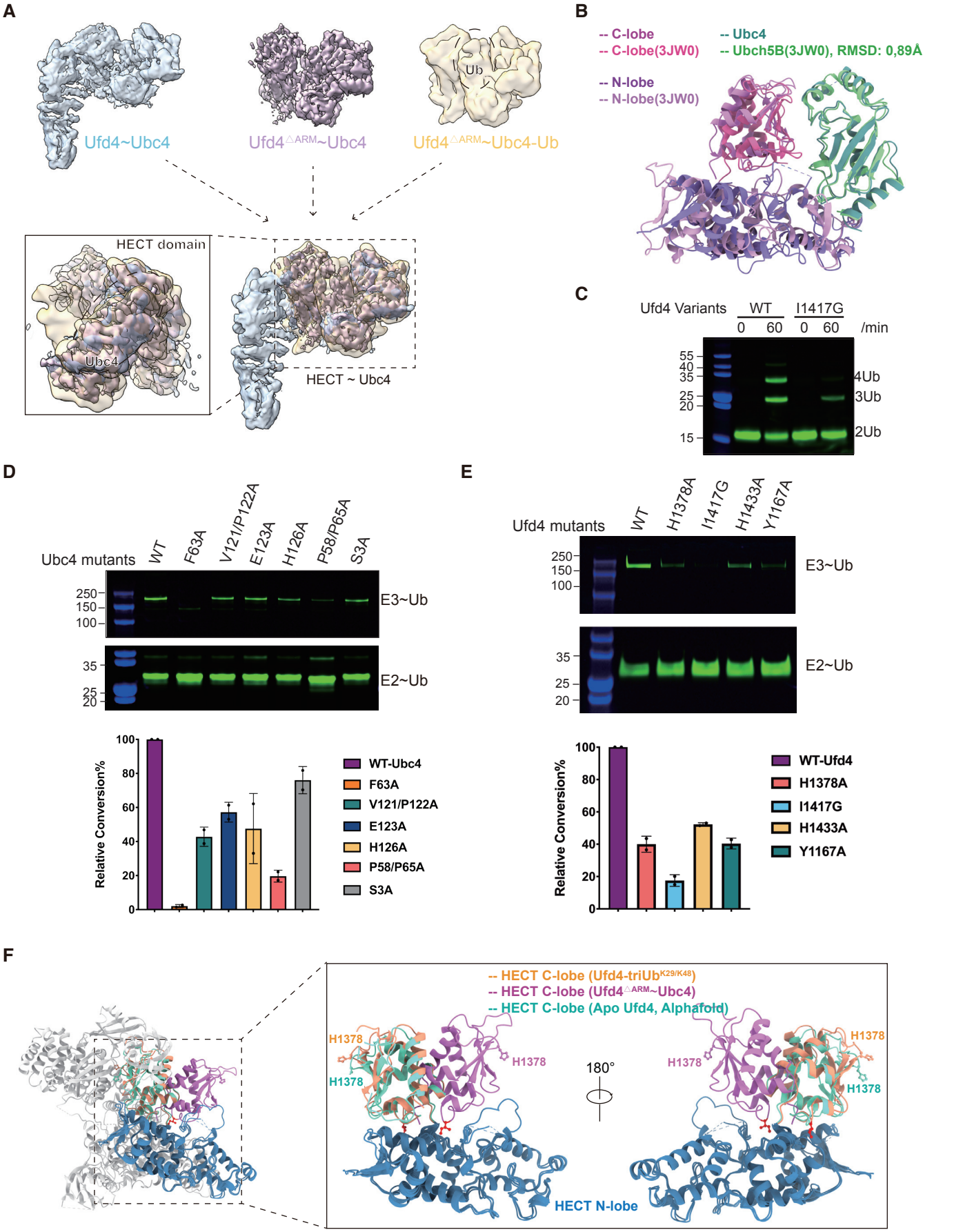

Figure S9: Analyses of the interfaces in Ufd4~Ubc4-Ub structure, related to Figure4

(**A**) Cryo-EM densities of Ufd4~Ubc4, Ufd4$^{\triangle ARM}$-Ubc4 and Ufd4$^{\triangle ARM}$-Ubc4-Ub and their structural alignment.

(**B**) A structure alignment of HECT domain-E2 determined in this study with HECT E3-E2 structure (3JW0). Root-mean-square deviation (RMSD) of backbone atoms are indicated.

(**C**) In vitro ubqituitination assay of wild-type Ufd4 and I1417G mutant.

(**D** and **E**) In vitro E3~Ub thioester formation assays. Mutations of Ubc4 F63A, V121A/P122A, E123A, H126A, P58A/P65A, S3A (**D**), and mutations of Ufd4 H1378A, I1417G, H1433A, H1433A/E1435A, Y1313A, Y1167A (**E**) are tested. Columns of relative conversions (%) are shown on the bottom.

(**F**) A structural alignment of the HECT domain in Ufd4$^{\triangle ARM}$-Ubc4, Ufd4-triUb$^{K29/K48}$ and Apo Ufd4 (predicted by Alphafold,AF-P33202-F1) structures. The HECT C-lobe in Ufd4$^{\triangle ARM}$-Ubc4 structure is colored in pink, in Ufd4-triUb$^{K29/K48}$ structure is colored in orange, in Apo Ufd4 is colored in turquoise Root-mean-square deviation (RMSD) of backbone atoms are indicated. Gel images and columns in **C**, **D** and **E** are representative of independent biological replicates (n = 2).

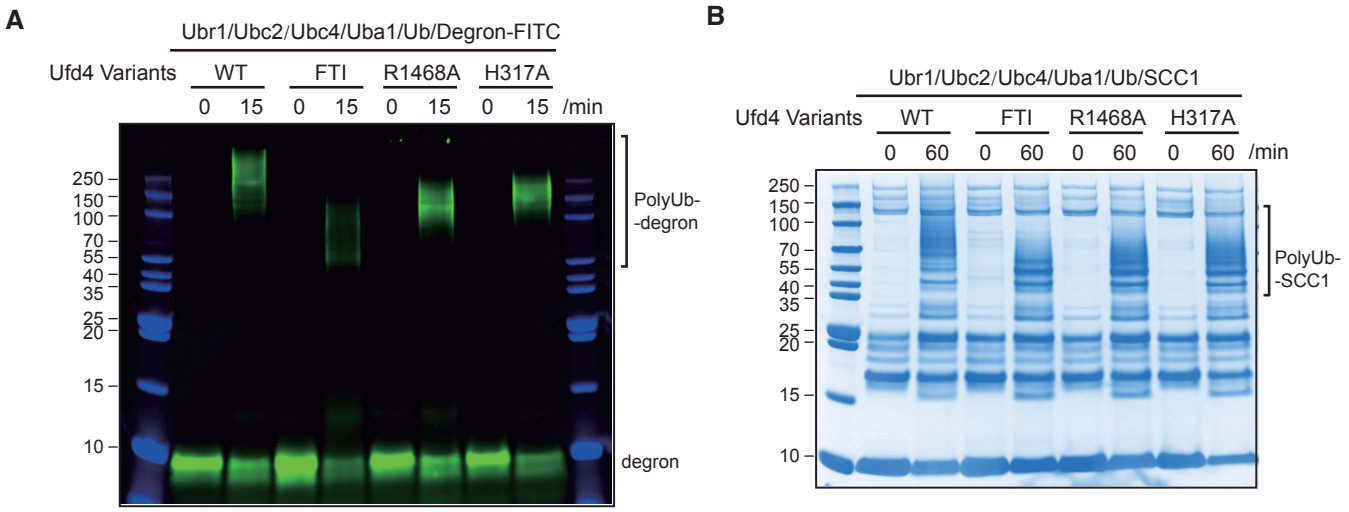

Figure S10: Ub chain assembly mechanism of Ufd4 and validation on other substrates, related to Figure3
(**A** and **B**) In vitro Ufd4- and Ubr1-dependent ubiquitination assays on degron (**A**) and Scc1$^{268-384}$ (**B**). Mutations of Ufd4 FTI (F313A/T315A/I316A), H317A, R1468A are tested.

Table S1 Cryo-EM data collection, refinement and validation statistics

	Ufd4 in complex with K29/48 triUb (EMD-35929, PDB:8J1P)		Ufd4 in complex with Ubc4-Ub (EMD-35931, PDB 8J1R)	
Data collection and processing				
Magnification	81,000		81,000	
Voltage (kV)	300		300	
Spherical aberration (mm)	2.7		2.7	
Detector	K3		K3	
Electron exposure (e^-/Å^2)	50.0 e^-, 32 frames		50.0 e^-, 32 frames	
Defocus range (μm)	–1.5 to –2.0		–1.5 to –2.0	
Pixel size (Å)	1.074		1.074	
Symmetry imposed	C1		C1	
Box size (pixel)	256		256	
Micrographs (no.)	5332		3404	
Initial particle images (no.)	5,926,009		2,011,193	
Final particle images (no.)	172,037		124,116	
Map resolution (Å)	3.31		3.52	
FSC threshold	0.143		0.143	
Model building and validation				
Initial model used	PDB: 1UBQ AlphaFold: AF-P33202-F1		PDB: 1UBQ, 1QCQ AlphaFold: AF-P33202-F1	
Model resolution (Å)	3.08	3.87	3.20	3.90
FSC threshold	0.143	0.5	0.143	0.5
Map sharpening *B* factor (Å^2)	-70		-80	
Nonhydrogen atoms	11523		6519	
Protein residues	1458		823	
Nucleotides	0		0	
Ligands	0		0	
Protein min/max/mean	30.00/244.58/132.28		30.00/226.74/122.51	
Ligand min/max/mean	---		---	
R.m.s.d. of bond lengths (Å)	0.003		0.003	
R.m.s.d. of bond angles (°)	0.812		0.712	
MolProbity score	2.06		1.86	
Clashscore	15.62		12.39	
Rotamer outliers (%)	0		0.14	
Cis proline/general (%)	2.1/0.7		5.4/0.3	
Twisted prolin/general (%)	0.0/0.1		0.0/0.0	
CaBLAM outliers (%)	3.18		1.40	
Favored (%)	94.71		96.26	
Allowed (%)	5.22		3.61	
Disallowed (%)	0.07		0.12	